Damage detection of composite materials via electrical resistance measurement and IR thermography: A review

Kundo Park[1], Junhyeong Lee[1], Seunghwa Ryu[1*]

[1]Department of Mechanical Engineering, Korea Advanced Institute of Science and Technology (KAIST), Daejeon 34141, Republic of Korea

Corresponding author:

*E-mail: ryush@kaist.ac.kr

Abstract

Composite materials, composed of multiple constituent materials with dissimilar properties, are actively adopted in a wide range of industrial sectors due to their remarkable strength-to-weight and stiffness-to-weight ratio. Nevertheless, the failure mechanism of composite materials is highly complicated due to their sophisticated microstructure, making it much harder to predict their residual material lives in real life applications. A promising solution for this safety issue is structural damage detection. In the present paper, damage detection of composite material via electrical resistance-based technique and infrared thermography is reviewed. The operating principles of the two damage detection methodologies are introduced, and some research advances of each techniques are covered. The development of IR thermography-based NDT including optical thermography, laser thermography and eddy current thermography will be reported, as well as the electrical impedance tomography (EIT) which is a technology increasingly drawing attentions in the field of electrical resistance-based damage detection. A brief comparison of the two methodologies based on each of their strengths and limitations is carried out, and a recent research update regarding the coupling of the two techniques for improved damage detection in composite materials will be discussed.

1. Introduction

A composite material is a combination of multiple constituent materials, that have quite dissimilar chemical and physical properties, in a particular microstructure to create an improved property unlike the individual components. It is different to chemical mixtures and solid solutions in that the constituent materials remain distinct within the overall structure and this micro-architecture takes an important role in the finished material properties. Although there exist various multiphysical and multifunctional applications of composite materials such as thermoelectric composites, sensors, and actuators, the composite materials are preferred in a wide range of industries mainly because of their outstanding mechanical properties; strength-to-weight and stiffness-to-weight ratio [1-3]. Their excellent mechanical properties extensively increased the demand of composite materials in various industries, such as buildings, automotive, and aerospace structures, rapidly replacing the use conventional materials. Especially for weight-sensitive industries, such as aircrafts, vehicles, and satellites, last decade has seen a dramatic increase in the use of fiber reinforced composites such as glass fiber reinforced plastic (GFRP) and carbon fiber reinforced plastic (CFRP) as they possess superior specific strengths and stiffness than conventional metal and alloys.

However, the microstructural complexity of composite materials not only resulted in their unique mechanical properties, but also made it difficult to predict their failure mechanism and residual material life. The heterogeneous and complex architecture inside composite materials led the overall structure to fail in a more complicated and diverse way, accompanying various possible failure phenomena, such as fiber rupture, fiber sliding, delamination, and interfacial debonding [4-6]. The failure modes of composite materials can be significantly different depending on the reinforcement architecture and type of external load applied, making it significantly challenging to theoretically predict its fracture properties. Especially for mechanical components under fatigue loads, which is a common industrial application of composite materials, the theoretical prediction of fatigue properties of composite materials remains as a daunting challenge when one thinks about the number and diversity of parameters that may affect the governing failure mechanism [7, 8]. Therefore, the application of composite materials in safety-critical structures, such as aircrafts and buildings, normally involve an undesired “overdesign” of the components in order to ensure a high safety factor against the failure of composites which we cannot predict [9, 10]. Overdesigning a structural component

not only increases the cost of material production and component construction, but it also makes it ineffective in exploiting the lightweight potential of composite materials, which is big advantage of using such materials.

Structural damage detection refers to a process of analyzing both internal and external damage of a structural component to diagnose the current state of material health. Non-destructive damage detection systems have been recently highlighted as a promising solution for the above-mentioned issues of composite materials [11-13]. In order to avoid overdesigning and ensure reliability at the same time, the formation of damages in the composite materials must be periodically monitored by the above-mentioned system and the detection of critical damage must be notified by the operator, so that corrective measures can be taken to stop the defects from evolving to a failure level. The identification of damage can be carried out without harming the structure being tested by a wide variety of non-destructive testing (NDT) systems, including radiographic testing, visual inspection, ultrasonic testing, infrared (IR) thermography testing, acoustic emission testing electromagnetic testing [14, 15]. Each of the testing methodologies has its own pros and cons in terms of detecting the formation of damage in a composite material, which is why it may require a combination of methods to ensure a success of evaluation.

Among the available non-destructive methods for structural damage detection of composite materials, this paper gives an overview of IR thermography and electrical resistance-based damage inspection. The principles of the two NDT will be introduced, and some of the recent research highlights associated with each of the two techniques will be reviewed. The recent development of IR thermography-based NDT including optical thermography, laser thermography and eddy current thermography will be reported, as well as the electrical impedance tomography (EIT) which is a technology increasingly drawing attentions in the field of electrical resistance-based damage detection. At last, the two methodologies will be compared based on each of their strengths and limitations, and a recent research update regarding the coupling of the two methods for improved damage detection in composite materials will be covered.

2. Infrared thermography-based damage detection

The first use of infrared wave based thermographic techniques for damage detection traces back to late 1970s, when the invention of infrared camera made it possible to qualitatively monitor the temperature field over a wide inspection area [16, 17] . The incessant development of technology associated with IR camera system has resulted in a the most advanced IR thermography, which allows us to obtain a highly informative thermal map that has excellent spatial resolution, thermal sensitivity, and frame rate. Thermal imaging has therefore gained a tremendous attention in a vast spectrum of commercial and industrial sectors. Thermal camera capacitates firefighters to detect people inside the heavy smoke and also to locate the base of a fire. Building construction specialists check the thermal signatures to localize the heat leakage spot in defective thermal insulation, and adopt appropriate measures to improve the efficiency of overall air-conditioning and heating system [18].

2.1) Theoretical principle of IR thermography

Infrared thermography is a technology of acquiring and analyzing thermal information of a surface or object in a contactless manner [19]. The scanning of temperature is possible by the principle that a grey body emits electromagnetic radiation in infrared range, that has a wavelength between 0.7μm and 1mm [20]. By exploiting its characteristic that the IR radiation strongly depends on the temperature of the emitting body, it is possible to measure the surface temperature of an object [21]. In order to perform thermal imaging based on the emitted radiation, IR camera performs a course of process which includes optical focusing of radiation, filtering of IR spectral band, detection of IR ray, conversion of the energy into electrical voltage, and processing of signal [22]. (Figure 1.a)

The intensity of radiation from a blackbody detected in the IR camera can be used to characterize the surface temperature by using the following relationship derived by Planck,

$$E_{\lambda b} = \frac{C_1}{\lambda^5 (e^{C_2/\lambda T} - 1)}$$

where $E_{\lambda b}$ is the intensity of black body radiation, $C_1 = 2hc^2$ and $C_2 = hc/k_B$ are the first and second radiation constants, λ is the wavelength of the radiation, T is the absolute

temperature of the black body [23]. The total hemispherical radiation intensity can be obtained by integrating the above equation over the entire spectrum ($0 < \lambda < \infty$),

$$E_b = \sigma T^4$$

where $\sigma = 5.670 \times 10^8 J \cdot m^2 \cdot s \cdot K^4$ is the Stefan-Boltzmann constant. Since the equations driven above are under the assumption that the radiation is emitted from a blackbody, the calculated intensity indicates the maximum intensity possible at a given temperature. Real objects, therefore, generally radiate only a portion of the ideal intensity $E_{\lambda b}$ under the same temperature and at the same wavelength condition. The concept of spectral emissivity coefficient ε_λ is adopted to account for this discrepancy, and the equation (1) can be rewritten for the intensity of real objects E_λ by multiplying this coefficient.

$$\varepsilon_\lambda = \frac{E_\lambda}{E_{\lambda b}}$$

Therefore, it can be noted that the intensity of radiation detected by the thermal camera is not only a function of temperature, but also a function of emissivity coefficient which depends on the type of material, the type of surface treatment applied, and even the temperature for some materials.

Another important factor that has to be taken into account is the surrounding environment under which the measurement is made. Depending on environmental parameters like air temperature and relative humidity, a portion of radiated energy may be absorbed by the atmosphere between the object and the camera, reducing the accuracy of absolute value of the measured temperature [24]. Concurrently, uncontrolled energy from surrounding that is reflected on the surface of the studied material may add undesired error to the measurement. To mitigate these systematic errors, the camera must be calibrated whenever its operating condition is changed. The calibration function suggested by Martiny, M., et al. has a similar functional form with Planck's law, and it relates the actual energy intensity to the surface temperature and to the emissivity coefficient through calibration coefficients A, B, and C [20, 25].

$$E = \varepsilon \frac{A}{e^{B/T} - C}$$

The value of the three calibration coefficients are empirically determined by the user through a blackbody experiment, and this calibration resulted in a reasonable approximation of temperature for a general measurement situation.

Regarding the application of IR thermography for the detection of damage in materials, an important quantitative analysis that can be conducted with IR thermography is the experimental measurement of material stress based on thermoelastic stress analysis [26, 27]. Thermoelastic effect is a thermomechanical theory that accounts for the reversible temperature change that occurs in a homogeneous isotropic material undergoing volume change due to external loading. This relationship between the stress state of a material and the temperature change is only applicable under linear elastic deformation and adiabatic condition.

$$\Delta \mathrm{T} = -\frac{\alpha}{\rho C_p} T_0 \Delta\left(\sigma_x + \sigma_y + \sigma_z\right)$$

T_0 Is the initial temperature, α is the coefficient of linear thermal expansion, ρ is the density, $\mathrm{C_p}$ is the specific heat capacity of the material, and the term related to the stress is the change in the first stress invariant. The reversible temperature change of a homogeneous isotropic material during its linear elastic deformation can be detected with IR thermography, and the value of temperature change allows us to calculate the stress state of the material. To expand the applicability of thermoelastic theory, some researchers extended the equation of thermoelectricity to orthotropic materials by taking the anisotropic thermoelastic constant into consideration [28]. Regarding composite materials, the relationship above does not hold in macro-scale as the heterogeneous structure consists of multiple materials with different material properties. But the theory allows us to understand the reason for the linear temperature reduction that is often seen in the early stage of composite deformation [29, 30].

While the elastic expansion of material is characterized by the reduction of temperature, irreversible formation of micro-damage in a material is generally represented by

the local increase in temperature [29-32]. As it can be seen from the Figure 1.b, various thermo-mechanical phenomena during the instant of damage formation result in an abrupt increase of local temperature allowing us to locate the onset of internal damage. At the moment of internal damage formation, the elastic energy stored in the material is rapidly converted into different forms of energy such as kinetic energy, sound energy, and heat. Especially for continuous fiber reinforced composites, the irreversible onset of internal damage accompanies rapid structural transitions such as crack formation, reinforcement-matrix debonding, and slippage of fiber, that brings about a local burst of frictional heat (Figure 1.b) [33]. At the same time, the stress relaxation near the micro damage also leads to a local increase in the temperature, as the removal of tensile thermoelastic effect makes the local field to recover its initial temperature.

2.2) Application of the technique for composite materials

Thermographic analysis can be applied in either active or passive mode: the former method employs an external source to add extra energy to the objective material whereas the latter monitors the temperature of an object without applying any external stimulus [30, 34]. For the active thermography, mechanical or thermal excitation source induce internal heat-flow inside the material to be studied, and allows us to monitor thermal peculiarities in the areas of cracks, voids, or other defects. On the other hand, the passive thermography is more suitable for monitoring dynamic change of temperature in the material instigated by real-time formation of internal damage. It has been demonstrated in numerous researches that various physical phenomena associated with internal defect formation, e.g. fiber breakage, fiber-matrix debonding, and delamination of plies in fiber reinforced composites, can be qualitatively observed with IR thermography [35-39].

2.2.1) Passive IR thermography

In passive thermography of composite materials, a material subject to static loading is monitored with an IR camera so that the dynamic temperature variations driven by the failure-related physical phenomena inside the material can be captured [31, 37]. During the static deformation of composite materials, various thermo-mechanical coupling phenomena can arise in the material, such as the thermoelastic effect, initiation of micro damages, fiber

breakage, fiber-matrix detachment, and delamination [4, 5]. Researches using passive IR thermography tried to capture aforementioned damage-related phenomena in various type of composite materials in diverse loading conditions [40]. Harizi, W., et al. tried to characterize the damage and thermomechanical behavior of GFRP with $[0°/90°]_s$ layers under static tensile loadings. Their thermal imaging analysis allowed qualitative evaluation of both the ply delamination and fiber-matrix debonding at high stress levels [37]. Libonati, F. and Vergani, L. used diagonally reinforced GFRP with ±45° layers of fiberglass to perform monotonic tensile test, and were successful in observing various thermo-mechanical behaviors throughout the deformation, which allowed them to divide entire deformation and failure process into three characteristic stages [26]. The first stage is characterized by a completely elastic behavior of the material, in which they observed a linear reduction in overall surface temperature that can be primarily explained by the thermoelastic effect. In the second and thirds stage, the temperature reduction deviated from the initial linearity due to irreversible micro-damage formation and propagation of crack, respectively (Figure 2.b). Detection of damage via IR thermography was also effective in carbon fiber reinforced polymers, which is one of the most commonly used lightweight structural composite material. Munoz, V., et al. used passive IR thermography to spot various damage mechanisms including matrix cracking, debonding, and fiber breakage during the uniaxial tensile test of $[0]_{14}$ and $[90]_{14}$ unidirectional CFRP (Figure 2.a) [38]. The passive IR thermography has shown its damage sensing capability in more complex geometry and loading condition in the research conducted by Zalameda, J. and W. Winfree [31]. They carried out a quasi-static 7-point load test with a hat-stiffened woven graphite epoxy composite panel, a structure that is commonly used in aerospace industry. With passive IR thermography, they could detect instantaneous temperature rise near the formation of damage, as well as the heating at the interface of failure. They also evaluated the time gap between the two types of temperature jump in order to deduce the depth of the damage.

2.2.2) Active IR thermography

While passive thermography is suited for monitoring of dynamic formation of defect, active thermography allows us to characterize the existing damages by applying various external stimulus to the inspected material in order to artificially induce temperature changes near the defects. One of the most common and conventional way of detecting internal damage is flash thermography, which typically applies a spatially uniform pulse of light with

xenon or halogen lamp [41, 42] (Figure 3.a). The high-energy heat pulse generated by the lamp is directed at the surface of the composite, and the thermal wave penetrates the material in depth and travels back to the surface. During this process, the temporal changes of the temperature recorded by IR camera is post-processed to obtain a contrast image of what is inside the material. Guillaumat, L., in his study, adopted a halogen lamp to introduce thermal excitation to the target material that has an initial delamination, and obtained a thermal cartography of the internal delamination via infrared camera [39] (Figure 2.c). With similar method, Toscano, C., et al. successfully diagnosed both slag inclusions and the percentage of porosity in CFRP plate with various stacking sequences [43]. An important advance in flash thermography was made by Poelman, G., et al in their recent study, where they overcame the limitation of flash thermography regarding the inspectable defect depth [44]. They introduced the concept of pulsed phase thermography (PPT) in which the phase images at different thermal wave frequencies are obtained and processed in order to significantly extend the depth of inspection.

For the last decades, ultrasonic IR thermography (UIT), also known as acoustic thermography, has been widely recognized as another important type of active thermography in various industries [45-47]. In case of ultrasonic thermography, mechanical excitation is accomplished by attaching an ultrasonic transducer to the surface of inspected material and applying continuous, modulated, or pulsed sonic excitations. The mechanical energy travels in the sample and is converted to heat in vicinity of the internal discontinuities, allowing us the detect the change in temperature near the defects. The exact mechanism of how the vibrational energy is converted into heat near the damaged spots is still a topic of discussion, and it is shown in relevant papers that the heat is generated due to some thermo-mechanical phenomena, such as plastic damping, thermoplasticity, internal hysteresis loss, and friction between cracked edges [35, 36, 48-50]. In the work of Rantala, J., et al., amplitude-modulated ultrasonic IR thermography was used to examine various damages in CFRP composite, and the result clearly illustrated some material discontinuities including voids and cracks [51]. Yang, B., and Y. Huang attempted to examine a composite material that is used as an actual wing rib of an unmanned aerial vehicle, and successfully spotted some impact damages [52, 53] (Figure 2.d). The strength of this methodology was that the end results of the inspection showed a high robustness against the position of the pulse injection point. Nevertheless, a main weakness of UIT is that, depending on the power of ultrasound applied, a new defect

may be introduced in the microstructure of material.

2.2.3) Advanced IR thermography

Nowadays, the IR thermography has evolved in diverse ways and newer techniques such as eddy current thermography [54-56], laser thermography [57, 58], and lock-in thermography [59] are gaining popularity. Figure 3.b illustrates the overall setup of an Eddy current thermography system, including inductive coil of wire, IR camera, eddy current generator, and data processing unit. Eddy current thermography, also known as induction thermography, applies a burst of electromagnetic wave to the material surface by placing the coil of wire that is excited with an alternating current of high frequency, thereby introducing eddy current into the objective material. By adjusting the excitation frequency, the user can control the depth of current flow inside the material, thereby allowing the user to search for the internal damage at desired depth. This depth of inspection is calculated as follows:

$$\text{depth} = \sqrt{\frac{2\rho}{\omega\mu}}$$

where ρ is the resistivity of the studied material, and $\omega = 2\pi f$ is the angular frequency of the eddy current, and μ is the permeability [60]. The current line induced in the material generally follow the shape of excitation coil in defect-free region, but the current line is distorted around the crack as it disturbs the flow of current in the component. The current density is higher at the crack tip and lower at the crack flanks. Due to the current field distortion at the damaged region, the joule heating effect associated with the eddy current flow causes different level of heat generation near the internal discontinuities. Although Eddy current thermography is only applicable to electroconductive materials, it is capable of detecting the defects in improved spatial resolution, frame rate, and temperature sensitivity compared to the conventional active thermographic methods [61, 62]. However, in case of fast inspection where we use the early thermal response, the detectable depth range of ferromagnetic materials is generally very small due to their high permeability, significantly limiting the internal damage detecting capability of Eddy current thermography. Wu, J., et al. recently proposed a DC-biased magnetization-based Eddy current thermography (DCMECT) in order to increase the penetration depth for the inspection of ferromagnetic materials [63]. To increase the thermal contrast between the intact and damaged region inside the material, DCMECT adjusts the permeability of material by exploiting the nonlinear magnetic permeability of ferromagnetic

materials.

Laser thermography is another promising thermographic method which is especially suitable for the damage sensing of joints, welds and thin films [64, 65] (Figure 3.c). In laser thermography, exposure to high energy laser stimulates heat flux in a defined area, and the temperature differences formed on the surface of the material due to the subsurface thermal barriers, i.e. defects, allows us to characterize the distribution of internal damage. Starting from a relatively small and selective region where the laser beam is applied, the heat conduction occurs in a symmetrical manner along the test surface if the exists no subsurface discontinuities. On the other hand, the internal defects cause disturbances in this flow symmetry and allow us to detect their presence by observing the temperature of heated surface. The advantage of using laser thermography is that the beam of laser allows the material to be heated in a very selective position and area, allowing us to have an in-depth analysis of a specific part. In addition to that, the beam of laser can cause a spherical flow of heat in the material to be tested, allowing the detection of internal defects in any orientation [64, 66]. The speed of inspection can be significantly improved by adopting laser line scanning thermography, in which a long laser line, instead of a laser spot, is applied to the material while still producing the defect images of similar qualities [67, 68]. Cerniglia, D. and N. Montinaro, in their recent study, highlighted the capability of laser thermography for the detection of near-surface defects in 3D printed metal component [69].

An important technique of choice regarding the reduction of statistical noise in the IR thermography is the lock-in method [70, 71]. The objective of the lock-in principle is to determine only the AC (alternating current) component of the detected signal, given the thermal excitation of the material is periodically pulsed or sinusoidally modulated in a certain frequency [72]. The periodic input energy wave can be provided with various excitation methods (i.e. ultrasound, eddy current, flash lamp) and it has to be modulated in a certain frequency called ‘lock-in frequency’, the optimal value of which depends on various conditions of evaluation such as thermophysical properties of the target object and the depth of evaluation. The input energy wave applied to the object penetrates the surface and travels in the direction normal to the surface. When the periodic input energy wave reaches the discontinuities inside the object, the wave is partially reflected back to the surface, allowing us to capture the temperature abnormality via IR camera. As it can be seen from the Figure 4, the key concept of lock-in correlation procedure in IR thermography is to multiply the detected IR images $F(t)$ by a set

of weighting coefficients $K(t)$ having a form of symmetric harmonic function with the lock-in frequency. By linear averaging of the processed signal S over a certain integration time t_{int},

$$S = \frac{1}{t_{int}} \int_0^{t_{int}} F(t)K(t)\, dt$$

If $K(t)$ is a symmetric harmonic function and if the integration time is a multiple of the period, the averaged value of $K(t)$ is equal to zero, hence suppressing the effect of random noise of the detected signal $F(t)$. In case of a digital lock-in correlation, the analog input signal $F(t)$ in the expression above is digitized into discrete numbers F_k, and the correlation procedure is performed numerically:

$$S = \frac{1}{M} \sum_{k=1}^{M} F_k K_k$$

The correlation function $K(t)$ is also replaced by a set of numbers K_k that follow a harmonic function, and their total sum must be zero in order to obtain an efficient suppression of random noise.

Since the amplitude and phase of the measured signal may be different in different pixels in the images, a lock-in correlation has to be performed with correlation functions with a phase difference, from which we can obtain both amplitude and phase image. Amplitude image is particularly effective in detecting a local heat source in an electrical component as the amplitude value is directly related to the locally dissipated power. On the other hand, the phase image is more applicable for the detection of internal defect as it depends heavily on the local IR emissivity.

3. Electrical resistance-based damage detection

The unique mechanical and electrical properties of carbon-based nanomaterials, including carbon nanotubes (CNT), graphene, carbon black, offered a considerable potential to the field of material damage detection. When uniformly dispersed in the matrix of a composite material, the carbon-based nanomaterials act as an excellent passive reinforcement that allows us to tune not only the mechanical properties, but the electrical properties as well. Baughman, R.H., et al. first exploited the electromechanical potential of CNTs by designing a conducting polymer actuator based on sheets of single-walled CNTs [73]. Carbon based nanocomposites have therefore gained a tremendous attention in various research fields, including electromechanical actuators, strain sensors, mass sensors [74]. Some of the recent reports have utilized the uniformly dispersed carbonaceous nanomaterials in a composite material to monitor, in a non-invasive way, the internal damage under static and dynamic loading condition [14, 29, 75, 76].

3.1) Dispersion of carbonaceous nanofillers in polymer matrix

Carbon nanomaterials can deliver superb multifunctional and mechanical properties to conventional composite materials when they are properly dispersed in the matrix [77-80]. Such benevolent influence of carbon nanomaterials is rooted from their own unique material properties and, thus, it is important to understand the material properties of the carbon nanomaterials. The mechanical and multiphysical properties of carbon-based nanomaterials including SWCNT, MWCNT, graphene, and fullerenes are summarized in Table 1. It can be seen clearly from the table that CNTs and graphene have advantages over graphite in their mechanical, electrical, and thermal properties due to its fundamental structure constructed with sp^2 hybridized bonds. Due to their unique properties, carbon nanomaterials have excellent potential for many industrial and engineering applications such as conducting plastics, robot skins, thermal conductors, energy storage, structural materials, lightweight materials, air and water filtration [81-83]. Despite these great potentials for carbon nanomaterials when properly embedded in a material, the real-life applicability of this reinforcement is significantly confined due to the dispersion problem. In order to achieve the effect of reinforcement with the carbon nanomaterials, it is crucial to disperse the nano-scale particle uniformly and homogeneously in the liquid-state matrix material before the addition of hardener. However, the carbon nanomaterial is literally a nano-scale material that has strong tendency to aggregate, particularly due to hydrophobic attractions and van der Waals attractions between the particles

[84-86]. Especially for CNTs having a high length-to-diameter ratio, the entanglement between the long fibers is another important factor that hinders the dispersion.

In mechanical perspective, an well-dispersed CNT of 0.5 wt.% in a polyvinyl chloride (PVC) matrix has proven to provide greater ultimate strength and failure strain compared to the same material with poorly dispersed carbon nanotubes [87]. Yazdani, H. who conducted this research added that this is possibly because the stress transfer between the nanomaterial and the matrix is significantly reduced when the carbon nanotubes are agglomerated into bundles. Li, J., et al. experimented the effect of carbon nanotube dispersion on the electrical property of the CNT-epoxy nanocomposite, by producing different dispersion states by adopting four different dispersion methods [88]. Percolation threshold is a terminology that refers to the minimum concentration of the conductive reinforcement needed to form a percolating, interconnected network in the host matrix. From their experiment, it is found that the percolation threshold varies from 0.1wt% to <1wt% depending on the dispersion technique used, which resulted in different dispersion states. This result allows us to understand that, even with a low loading of carbon nanomaterials, a percolating electrical network can be formed inside the host polymer if the reinforcing particles are thoroughly dispersed.

In order to dope the host matrix of a composite material with carbon nanomaterials, powder-like nanomaterials must be added to the liquid-state matrix material before the addition of hardener. To uniformly disperse the nano-sized particles in the solution, various physical blending techniques have been adopted in existing researches regarding the carbon-based nanocomposites. One common approach is to use calendering technique, in which the mixture is repeatedly passed through number of pairs of rolls until it reaches high degree of nanotube dispersion [29, 75]. Chang, L., et al. applied different rolling speed to each of the rolls and allowed only a small gap between the rolls in order to induce significant shear forces, which effectively disentangled the agglomerates with limited breakage of nanotubes [89]. High power dispersion methods, including ultrasound and high-speed shearing, can also be convenient options. Tip sonicator is a typical equipment that is used to deliver vibrational energy to the mixture and induce homogeneous dispersion of CNTs [90]. Qian, D., et al. applied high energy sonication to prepare a uniformly dispersed polystyrene/MWCNT mixture that is later hardened into a nanocomposite film [91]. Sandler, J., et al., on the other hand, adopted high speed stirring in 2000rpm for 1 hour and showed that this straight forward blending technique is also an effective way to achieve a uniform dispersion of CNT in epoxy resin [92].

To further stimulate the dispersion and even achieve stabilization of carbon nanomaterials, there have been research regarding chemical treatment of the nanomaterials [93-95]. It has been a major challenge to overcome the propensity of nanomaterials to agglomerate when dispersed in liquid phase matrix materials or fluids such as water and acetone due to their hydrophobicity and van der Waals attraction. For this issue, researchers tried to provide slight modification to the surface of the nanomaterials by attaching functional entities in order to change the hydrophobic nature of nanomaterials to hydrophilic one, which is a process called chemical functionalization. In direct covalent functionalization of CNTs or graphene, some of the sp^2 hybridized bonds are broken and changed into sp^3 hybridized bonds by linking carboxyl (COOH), hydroxyl (OH), or amino functional group. The functionalization process is normally carried out by allowing the nanomaterials to react with some highly reactive molecules, such as fluorine. The chemical bonding between fluorine and a purified single-walled CNT is known to occur at the temperature of 325℃ [96]. Then, a mixture of high concentration of additional functionalization agents, such as sulphuric acid, nitric acid, or hydrochloric acid, is added to replace the weak C-F bonds by other functional groups such as amino, alkyl, or hydroxyl groups [97, 98]. There are numerous alternative functionalization methods other than the fluorination, including cycloaddition, carbene and nitrene addition, chlorination, bromination, and hydrogenation, and they have all shown their potential in recent studies [99-101].

This chemical treatment of the nanomaterial improves both stability and dispersion of the nanofluid by inducing the electrostatic repulsion between the particles that diminishes the effect of van der Waals attraction, and making them hydrophilic in the base fluids. This repulsive effect helps the nanomaterials, especially carbon nanotubes, to become unbundled and deagglomerated. In a research conducted by Mitchell, C.A., et al., they prepared unfunctionalized single-walled carbon nanotube and 4-(10-hydroxydecyl)benzoate functionalized single-walled carbon nanotube and compared the quality of each groups' dispersion in polystyrene [102]. The resultant nanocomposite showed a percolation threshold of 1 vol% for the functionalized carbon nanotube, while the percolation occurred at twice nanotube loading for the unfunctionalized case. Chemical functionalization of nanomaterials can also improve the mechanical properties of the resultant nanocomposites by producing a strong interfacial bond between the nano-reinforcement and the matrix [93]. The aromatic nature of the molecular structures of CNT and graphene makes them chemically stable, thereby making themselves to interact with the host matrix mainly through van def Waals interaction which is not strong enough to bring about an efficient load transfer between the two phases. In

case of functionalized nanomaterials, the functional groups attached to the molecular surface allows the particle to produce strong interfacial bonds with the surrounding matrix, thereby better exploiting its excellent load bearing capacity as a reinforcement.

However, there still exist some inevitable adverse effects of chemical functionalization. Firstly, the breaking of planar sp^2 hybrid structure for the addition of functional group leads to the formation of defects and results in a reduced electrical conductivity of the nanomaterial. In the work of Loh, K.P., et al, the electrical conductivity of a nonfunctionalized graphene was higher than that of the functionalized ones, as the functionalities on the surface disrupted the mobility of electrical carrier [103]. Regarding the mechanical properties, the unrivaled mechanical strength and failure strain of carbon nanomaterials is not fully exploited under the presence defects in its lattice structure. In addition, the highly reactive chemicals used for the functionalization may lead to the fragmentation of the nanomaterials into smaller pieces [93].

3.2) Theoretical principle of electrical resistance-based damage detection

Once the dispersion and stabilization of carbon nanoparticles in the liquid state matrix is achieved through the above introduced physical and chemical procedures, the solidification of this mixture must be followed. The time required for this curing process to be complete depends on various factors including the type of resin used, the type of hardener used, the resin/hardener mass ratio, and the temperature at which the solidification takes place [104, 105]. In most cases, it is preferable to speed up the solidification process as the dispersion state of the nanomaterials in the mixture gradually deteriorates in its liquid phase due to the propensity of nanoparticles to re-agglomerate and even be deposited. Choosing an appropriate combination and mass ratio of resin/hardener is, therefore, an important stage that requires careful consideration as the solidification time depends tremendously on them. Another commonly adopted strategy to speed up the solidification process is to elevate the curing temperature, as the crystallization reaction of resin and hardener is accelerated by applying external heat. Once the curing of the mixture is complete with a high degree of nanoparticle dispersion, the electrically conductive network is established in the composite material.

The electrical resistance measurement of the conductive nanocomposite is carried out by introducing two electrodes on the sample with sufficient distance between them (Figure 7.a). The electrical conduction in the percolating network occurs in two different modes, i.e., the

intrinsic electrical conduction of nanoparticles and the contact of different nanotubes [106]. Regarding the first mode, for instance, the electrical conductivity of a common multiwall CNT is in the order of 10^6-10^7S/m, meaning that the carbonaceous nanoparticle itself is an excellent medium of electrical conduction [107]. The electrical conduction between two separate particles is more complicated as the quantum tunneling effect at a contact point may vary with numerous factors including nanoparticle diameters, tunneling gap at contact points, the matrix material that separates the nanoparticles [106]. Recent studies indicated that this contact resistance is the dominant factor that determines the overall electrical resistance of the percolative network [108]. The percolative network of carbonaceous nanomaterials in the composite material allows the user to monitor the formation of internal damage as the overall resistance of this network depends tremendously on such factor. As the sizes of nanoparticles are extremely small compared to the size of microscale cracks, the onset of damages or microcracks in the matrix breaks some of the conducting pathways in the percolating network, which leads to an increase in electrical resistance of the overall material (Figure 5). By monitoring the electrical resistance of the target material and comparing the value to the initial reference value, the user can readily detect the formation of material damage, and this in-situ nature of electrical resistance-based technology makes it a promising candidate for structural health monitoring in various industries and research fields.

The electrical noise is one of the important issues that has to be taken care of during and after the electrical measurement. There can be multiple sources in the system that causes this measurement noise, e.g., unstable electrodes, the reliability of the signal acquisition device, and the high sensitivity of the target material [109]. The systematic noise associated with the unstable connection of electrodes usually occurs when the electrode is built on the surface of the target material by attaching the electrical cable with the aid of various conductive adhesives such as silver pastes and aluminum tapes. This surface-mounted electrode generally shows poor robustness because the cable is not firmly fixed in its position while even a slightest movement of the cable may significantly change the measured voltage. The stability of electrical connection can be significantly improved by embedding the electrode inside the material, by submerging the conductive wire or thread into the liquid-phase material before the solidification stage [110, 111]. However, if excessive volume of conductive wire is introduced inside the material, the volume occupied by the wire can provide adverse effect on the mechanical stability of the material as it technically is an internal discontinuity.

The suppression of random noise in the acquired signal is also an important procedure as there exists multiple sources of random noise, including the signal generation device and signal processing device. In the electrical resistance measurement for the detection of damage, a careful selection of electrical current value can be an effective strategy to increase the signal-to-noise ratio. Based on the measuring conditions such as the conductivity of the fabricated sample, the maximum voltage of the power supply, and the voltage measurements on different electrodes, Baltopoulos, A., et al. chose to apply only a small amount of input current for the electrical measurement, and this this successfully increased the signal-to-noise ratio over 50dB for the voltage measurement [112, 113]. Another common way to deal with the high frequency random noise in the signal is to adopt low pass or band pass filter. Park, K., et al. adopted Savitzky-Golay finite impulse response filter to suppress the high frequency random noise components in their measured signal, so that they can focus better on the electrical signal associated with the structural damage [29].

Regarding the amount of conductive nanoparticle required to make the host material electrically conductive, the composite undergoes an insulator-to-conductor transition when the conductive nanoparticle content is gradually increased (Figure 6). At the percolation threshold, which refers to the minimum amount of conductive nanoparticle required to form a conducting network, the electrical conductivity of the nanocomposite sharply increases in several orders of magnitude. In case of conventional carbonaceous nanocomposites such as carbon black, exfoliated graphite, and chopped carbon fibers which are usually in micrometer-scale size, the percolation threshold is as high as 10-50 wt.% [114-116]. This excessive doping of filler can significantly degrade the mechanical properties of the end product, while increasing the manufacturing cost at the same time. Carbonaceous nanomaterials, including CNTs and graphene, gained a considerable interest as a promising solution for the aforementioned issues regarding the percolation threshold. Their unique properties, i.e. small size, high aspect ratio, and high electrical conductivity, made it possible to form a conductive percolation network inside a matrix at a dramatically lower filler content, often as low as 0.5 wt.% for CNTs.

Regarding the percolation threshold value of different carbonaceous fillers, there is no precisely defined values reported for each type of fillers as the establishment of conducting network depends not only on the amount of conductive fillers added, but also on various other factors including dispersion state, chemical treatment applied to the fillers, and the processing techniques adopted to produce the nanocomposites. In case of CNT/epoxy nanocomposites, the

percolation threshold values have been reported to vary from 0.002 to over 7 wt.% depending on the nature of CNTs (single-walled or multi-walled), the alignment of nanotubes, and the type of fabrication process used to produce the nanocomposite [88, 117-119] (Figure 6.b). Bauhofer, W. and J.Z. Kovacs compared the relative importance of various factors that affect the percolation threshold of CNT in their research, and concluded that the dispersion state of CNT was the most critical one over other factors such as type of CNT and production method of CNTs [120]. In their study, a well-dispersed CNT resulted in 50 times higher conductivities compared to the entangled CNT.

3.2) Application of the technique on composite materials

3.2.1) CNT-doped nanocomposites

Researches using CNT network-based damage detection tried to validate the applicability of the methodology in various loading conditions. Park, K., et al. attempted to detect the onset of micro-defects in a CNT-doped GFRP specimen with stacking sequence of [0°/45°/90°/-45°]2S under static tensile test [29]. As it can be seen from the figure 10.b, negligible change in electrical resistance was seen during the early linear elastic deformation mode. As the applied load becomes greater and starts to induce irreversible micro-damages in the material, the electrical resistance curve obviously starts to rise as the onset of damages interrupt the conductive percolation network. Thostenson, E.T. and T.-W. Chou applied the same technique on a GFRP under cyclic loading, and compared the strain-time graph with the electrical resistance graph to characterize the accumulation of internal damage [75]. They also performed non-linearity analysis on the electrical signal to determine whether the increase in electrical resistance indicate the re-opening of existing crack or a formation of a new crack (Figure 7.b).

The damage detecting efficiency of fiber reinforced composites with uniformly and non-uniformly dispersed CNTs has been compared in the study conducted by Gao, L., et al [121]. Calendaring technique was adopted to obtain a highly uniform dispersion of nanotubes in the resin matrix, while a non-uniform dispersion of nanotubes was achieved by using a nanotube that contains fiber sizing agent. They experimentally confirmed that the a highly uniform network yields in much higher sensitivity in terms of micro damage detection. Gao, L., et al also used electrically conductive network to detect the internal damage accumulation

under impact loading [76] (Figure 7.c). The electrical resistance of the CNT-doped epoxy/plain woven glass fiber composite increased with repeated impact loading, allowing the user to monitor the structural health in real time.

3.2.2) Graphene-doped nanocomposites

The manufacturing of graphene-based nanocomposites not only requires that graphene sheets be homogeneously distributed and incorporated into the host matrices graphene sheets, but that the nano-scale graphene sheets also be produced on a sufficient scale. While the production of thin graphene sheets can be started from graphite, which is an inexpensive carbonaceous material available in large quantity, the exfoliation process of separating the combined layers into individual graphene sheets has been a tough nut to crack. Stankovich, S., et al. presented a general approach for the preparation of graphene-polymer composite via ultrasonic exfoliation of graphite, and molecular-level dispersion and stabilization of individual graphene sheets within the polymer matrix by chemical means [122]. In this research, a polystyrene-graphene nanocomposite was formed with their fabrication process and it exhibited an electrical conductivity of $\sim 0.1\ \mathrm{S\ m^{-1}}$ at a percolation threshold of 0.1 vol.%. In a research conducted by Zha, J.-W., et al, a piezoresistive strain and damage sensor was developed by dispersing 1.31 vol.% of amino-functionalized graphene nanoplates in an epoxy matrix [123].

The internal damage detection of composites via graphene is generally carried out by introducing a thin film of graphene-doped layer into the non-conducting composite materials. One common way to introduce this thin film sensor to the composite material is to coat the surface of reinforcing fibers with the graphene. Balaji, R. and M. Sasikumar measured the accumulation of both strain and damage in a glass fiber reinforced polymer composite by embedding a single strand of fiberglass coated with reduced graphene oxide [124]. In a subsequent research where all of the reinforcing fiberglass are coated with graphene through electrophoretic deposition (EPD) process, it was shown that highly sensitive detection of both strain and damage was possible [125]. In addition, the author highlighted that, when deposited on the surface of glass fibers, graphene coated fibers outperformed the CNT coated fibers by showing higher sensitivity to strain and internal damage. The reason for this difference is that the graphene has a plate-like structure that can be readily adhered to the surface of glass fiber

and form a full coverage of surface, while CNTs are one dimensional material that can only touch each other by point-to-point contact. Alternatively, a graphene doped thin film interlayers can be built between the plies of common composite laminate structure. In the work of Groo, L., et al., they embedded laser induced graphene layer into fiberglass-reinforced composite and aramid fiber-reinforced composite by transfer printing the surface of the prepregs with graphene before being laid up into a ply stack [126, 127]. By this method, they could develop multiple piezoresistive interlayers between the plies, which showed both strain and damage sensing capability in three-point bending tests and uniaxial tensile tests.

3.2.3) Other conductive fillers

The insulator-conductor binary mixture can be formed with other carbonaceous nanoparticle fillers as well. Carbon black, having a form of paracrystalline carbon that has high surface-area-to-volume ratio, is a carbonaceous material that is mainly used as a reinforcing filler in tires and other rubber products to improve their tensile strength and wear resistance [128, 129]. In the research fields regarding the damage detection for composite materials, numerous studies used carbon black as a conductive filler to establish conductive network in a composite material, due to its graphite-type crystalline structure that provides an excellent electrical conductivity. Vadlamani, V.K., et al. generated a conductive network in epoxy resin with 10 wt.% of carbon black, and determined the electrical resistance changes associated with the deformation, damage initiation, and the growth of damage [130]. The applicability of carbon black as a conductive filler was extended in a research by Tallman, T.N., et al., where they adopted electrical impedance tomography to accurately determine the locations of multiple through hole defects in carbon black-doped fiberglass/epoxy laminates [131]. Here, electrical resistance tomography, which will be discussed further in the next chapter, refers to an electrical resistance-based technique in which the electrical resistance is evaluated at multiple locations to estimate the location and size of damage formation. Yazdani, H., et al. evaluated the damage detecting capability of the carbon black network in a polyvinylchloride matrix under cyclic loading condition [132]. Five different cyclic loading conditions were designed by diversifying the strain magnitude, loading rate, and prestraining conditions, and demonstrated the damage detecting capability of carbon black based multifunctional composite. Despite all the prospective research results associated with the carbon black as a conductive filler, it is generally less preferred than CNT and graphene due to their high percolation

threshold, as excessive doping of filler may deteriorate the mechanical property of the host material.

Carbon nanofiber, having a cylindrical nanostructure that has graphene layers arranged as stacked cones or plates, is also a feasible option as a multifunctional additive filler. Although this material has a diameter that is several orders greater than that of CNTs, the high length-to-diameter ratio which is a common feature that they share makes both of them a promising filler particle for continuous conducting network. Wang, Y., et al. performed both static and cyclic tensile test on a carbon nanofiber embedded GFRP with a nanofiber content of 0.86 wt.%, and demonstrated the in-situ strain and damage monitoring capability of this material [133]. Another research in similar context has confirmed that the carbon nanofibers-doped basalt fiber reinforced polymer laminates also have a great sensitivity in monitoring of the onset of internal damages under static and cyclic tensile tests [134]. Employment of carbon nanofibers showed its damage sensing capability even under impact test, where the filler is added to a glass fiber reinforced polymer laminates [135].

3.3) Electrical impedance tomography (EIT)

The researches discussed above have shown that the electrical resistance of the carbon-based nanocomposites increases with the formation of internal damage. However, practical structural health monitoring is interested in not only sensing that damage has occurred, but also in knowing the location of damage. In the early researches aimed at locating the damage, researchers instrumented a composite plate with multiple electrodes to partition the plate [136, 137]. Then, they examined the change in resistance of each partition in order to identify where the onset of defect has occurred. Although this approach has shown the ability to locate damage in carbon-based nanocomposites, too many electrodes were required to precisely characterize the location of damage.

Electrical impedance tomography (EIT) is a more sophisticated electrical resistivity-based imaging technique that potentially allows the user to monitor the damage map of a multi-dimensional material in real-time [138, 139]. Electrodes are built onto the material to be imaged usually along its periphery. A pair of electrodes are initially selected as an entrance and exit for electrical current, while voltages are measured between the remaining electrode pairs (Figure 8). Then the current is injected and extracted between the next electrode pair, and the voltage

is again evaluated between other electrode pairs. This process of data collection is repeated until all electrode pairs are injected with electric current and the voltage data set of every possible case of measurement is obtained.

To reconstruct the internal resistivity (or conductivity) using the EIT method, a forward problem and an inverse problem need to be solved. First, the forward problem estimates voltage on the domain from three given values: conductivity field of the material domain, the number of electrodes, and the current put in. The existence and uniqueness of the voltage solution have been proved for several forward models including the widely used complete electrode model [140]. Second, the inverse problem reconstructs the internal resistivity distribution from the voltage measurement and current stimulation data on the boundary electrodes. Likewise, the distribution of conductivity in the domain is uniquely determined when an infinite number of electrodes covers the entire boundary and current stimulates whole electrode pairs in sequence [141]. However, in practice, the number of the electrodes is finite, thus the resistivity in the body is approximated by a finite element method [142].

Mathematical formulation of EIT

This part describes a mathematical formulation of the forward problem and the inverse problem of the EIT. From the Maxwell equation, the equation (3.1) can be acquired as

$$\nabla \cdot (\gamma(x, \omega)\nabla u(x, \omega)) = 0 \tag{3.1}$$

where γ is an admittance field and u is a potential field on a given domain. The parameter ω is an angular frequency of injected current and x is a position on the domain. The admittance γ is the reciprocal of impedance. The real part of the admittance is the conductivity σ and the imaginary part is a permittivity ε. In the field of SHM, researchers usually focus on the reconstruction of resistivity by injecting direct current. For resistivity, the equation (3.1) is reduced to the equation (3.2).

$$\nabla \cdot (\sigma \nabla u) = 0 \tag{3.2}$$

It is notable that the equation (3.2) is analogous to a time-invariant diffusion equation.

In practice, a current is injected through a finite number of electrodes. Therefore, a mathematical model is required to describe the electrical properties of the electrodes and the material. Among assortments of models, the complete electrode model (CEM) is widely employed to solve the forward problem. The CEM gives boundary conditions (3.3) – (3.5) to the equation (3.2).

Electrode Voltage $$u + z_l \sigma \frac{\partial u}{\partial n} = V_l \quad on\ e_l, \qquad l = 1,2,3, \dots, L, \tag{3.3}$$

Electrode Current $$\int_{e_l} \sigma \frac{\partial u}{\partial n} dS = I_l \quad on\ e_l, \qquad l = 1,2,3, \dots, L, \tag{3.4}$$

Non- Electrode Boundary $$\sigma \frac{\partial u}{\partial n} = 0 \quad on\ the\ boundary\ between\ electrodes \tag{3.5}$$

Here, z_l is a contact impedance of each electrode, and $\frac{\partial u}{\partial n}$ is a directional derivate of the voltage u along with the outward unit vector n. V_l and I_l respectively denote the voltage and the current on the lth electrode of which surface is e_l. By applying the CEM to the equation (3.2), a solution is unique up to the addition of constant. To resolve this redundancy, two additional constraints (3.6) and (3.7) are applied [140]:

$$\sum_{l}^{L} I_l = 0 \tag{3.6}$$

$$\sum_{l}^{L} V_l = 0 \tag{3.7}$$

Then, the non-linear mapping F, the so-called forward model, correlates the voltage u and the conductivity σ as below

$$\mathrm{u} = \mathrm{F}(\sigma) + \epsilon \tag{3.8}$$

where ε is a zero-mean noise vector.

The inverse problem in EIT estimates the conductivity distribution based on the voltage measurement on the boundary and current stimulation. In other words, the inverse problem is finding the conductivity map in the domain minimizing the difference between experimentally measured voltage data and calculated potential from the forward model. In the form of an equation, the inverse problem written as

$$\sigma = \min_{\sigma}(\|V_m - F(\sigma)\|^2) \tag{3.9}$$

where V_m is the measured voltage and $\|\cdot\|$ is an appropriately defined norm, usually L2-norm.

The inverse problem solving the equation (3.9), quantitatively estimating the value of conductivity, is called abstract imaging. However, pragmatically, conductivity change is usually more crucial information than the absolute value. A small perturbation on the conductivity brings about a minute change of voltage on the electrodes, and this correspondence can be described by Taylor expansion:

$$\delta V = \left.\frac{\partial F}{\partial \sigma}\right|_{\sigma=\sigma_0} \cdot \delta\sigma = J \cdot \delta\sigma \tag{3.10}$$

J is Jacobian matrix, $\delta V = V_m - F(\sigma_0)$, and $\delta\sigma = \sigma - \sigma_0$. Thus, the inverse problem for the sufficiently small change of conductivity is expressed as below.

$$\delta\sigma = \underset{\delta\sigma}{\operatorname{argmin}}(\|\delta V - J\delta\sigma\|^2) \tag{3.11}$$

A qualitative estimation of the conductivity change by solving the equation (3.11) is known as difference imaging. The difference imaging is advantageous in an immediate detection of the electrical property change in the domain instead of handling an iterative procedure to solve the non-linear inverse problem.

The least square (LS) method (3.12), minimizing projected error-norm onto the solution space, is improper to this problem because of ill-posed characteristic of Hessian matrix $J^T J$.

$$\delta\sigma \cong (J^T J)^{-1} J \cdot \delta V \tag{3.12}$$

Due to the singular nature of the Hessian, the inverse problem needs to add a regularization term. The regularization method can be selected arbitrarily and judiciously by the researchers [143]. However, there are several typical ways in choosing the regularization term: researchers can adopt the commonly used ways such as Tikhonov [144], NOSER [145], and Laplace [146]. For instance, Tikhonov regularization is one of the most widespread methods that yield the approximate solution as the equation (3.13)

$$\delta\sigma \cong (J^{\mathrm{T}} J + \alpha^2 L^T L)^{-1} J^T \delta V \tag{3.13}$$

where L is a regularizing operator. For weighted least square methods with the weight matrix W, the equation (3.13) is modified to

$$\delta\sigma = (J^T W J + \alpha^2 L^T L)^{-1} J^T W \delta V \tag{3.14}$$

For the given error model ε in the equation (3.8), it is known that the weighted LS is the best linear unbiased estimator minimizing the total variance of the conductivity change when $\mathrm{W} = \mathrm{C_e^{-1}}$, where C_e is a covariance matrix of the zero-mean noise ε [147]. The following equation is the inverse problem in EIT considering both regularization and error effects.

$$\delta\sigma = (J^{\mathrm{T}} C_e^{-1} J + \alpha^2 L^T L)^{-1} J^T C_e^{-1} \delta V \tag{3.15}$$

As shown above, the inverse problem is a kind of optimization problem, thus researchers have tried to apply optimization algorithms such as genetic algorithm [148], particle swarm algorithm [149], and differential evolution [150, 151] to solve the problem. Furthermore, recently, ML algorithm has been adopted as an effective tool to find the conductivity solution [152-154].

Application of EIT to Structural Health Monitoring

Following researches adopted electrical impedance tomography (EIT) methods to detect a failure of composite materials such as cementitious or structural materials, carbon-based composites, and 3D-printed structures.

(1) Detection of damage on cementitious or structural materials

Hou, T.-C. and J.P. Lynch applied EIT to measure conductivity drop due to crack formations under tensile loading and three-point bending loading [155]. The author conducted the tensile loading and bending tests, by attaching 32 copper electrodes on the sides of the cementitious structure, and identified that this approach is suitable for damage characterization. Hallaji, M. and M. Pour-Ghaz conducted a four-point bending experiment with a silver-painted concrete and successfully localized rupture of the material using a difference imaging method [156]. In their following research, Hallaji, M., A. Seppänen, and M. Pour-Ghaz reconstructed the conductivity map of a copper-painted concrete beam utilizing an abstract imaging method, thus quantified the localized conductivity drop caused by the cracks on the material under four-point bending [157]. Rashetnia, R., et al. improved the accuracy of EIT in detecting a cracking pattern of a large reinforced concrete beam by installing internal electrodes [158].

(2) Detection of damage on carbon-based composites

Tallman, T.N., et al. adopted EIT for damage detection in carbon nanofiber filled epoxy nanocomposite, by building 16 electrodes along the periphery of the material (Figure 9.b) [159]. The author artificially induced a macro-scale damage in the material by drilling a hole, and successfully obtained a two-dimensional damage map that illustrated the correct location of the damage. The author, in his next research, extended the applicability of EIT on self-sensing material by introducing different type of damage [131]. An impact damage was applied and multiple holes were drilled on GFRP with carbon black filler, and electrical impedance tomography demonstrated its capability to visualize such damages in the material (Figure 9.c). Lestari, W., et al detect spontaneous defects caused by quasi-static tensile test on unidirectional glass fibered-reinforced polymer composites (GFRP) and plain-woven carbon fiber reinforced polymer composites (CFRP) by utilizing ERT [160]. The author installed 16 electrodes on the boundary of the materials and qualitatively reconstructed the conductivity in the domain using

a maximum *a posteriori* method.

Hou, T.-C., K.J. Loh, and J.P. Lynch imaged structural defects in the carbon thin film, fabricated via the layer-by-layer technique, based on the two-dimensional EIT method. The author also observed the film's response to the various pH circumstances using the electrical modality [161]. In the following research by Loh, K.J., et al, a CNT-polyelectrolyte sensing skin was fabricated via the layer-by-layer technique and attached to a metallic substrate [162]. Application of EIT on this sensing skin made it possible to monitor not only the strain, but also the onset of damage in the substrate material.

As the 3D printing technique develops, recently, researchers adopted EIT to reconstruct the conductivity of 3D-printed carbon composites. Ghaednia, H., et al. manufactured a 3D-printed specimen of the joint replacement using CF/PMMA and observed failure of the joint model under compressive loading using EIT [163, 164]

(3) Prediction of material failure

The study by ZHAO, Y., S. GSCHOSSMANN, and M. SCHAGERL compared the stress field of inkjet-printed CNT thin films obtained from two different methods: DIC and EIT. The study reveals that the EIT's potential in estimating crack severity and plastic zone near the crack tips is promising [165]. Hassan, H. and T.N. Tallman estimated displacement field of CNT/Epoxy specimen from a reconstructed conductivity map and a given analytical piezoresistivity model correlating strain and conductivity of the material [166]. The author acquired the stress field from constitutive equations with known Young's modulus and Poisson ratio. Then, the author predicted the failure of the specimen based on a simple criterion comparing the first principal stress near the hole and failing stress.

4. Coupled health monitoring system

4.1) Strengths and weaknesses of the two techniques

Each of the IR thermograph and electrical resistance measurement has its own strengths and limitations as a material health monitoring technique. The greatest advantage of

using IR thermography over other NDT techniques is its ability to inspect a relatively large area within a short time and clearly illustrate the location of damage formation in a thermal image [167, 168]. Thanks to the development of IR camera, real-time imaging of a material surface over a few m^2 became possible these days, and this technological leap broadened the applicability of IR thermography-based damage inspection in various industries. Another strength of this technique its adaptability regarding the type of target material. If an optimal excitation technique is adopted and appropriate 'black painting' procedure is taken, thermography is capable of inspecting a wide range of materials. Due the wide span of target material, IR thermography is the only possible inspection tool for some materials (e.g. some ceramic surfaces that are hardly examined by other inspection tools). However, proper inspection of internal damage is not possible with IR thermography if the studied material has a considerable thickness. In case of a damage formation that occurs deep inside a thick material, the heat induced near the damage formation is diffused in all direction and in a large volume of material. Since IR thermography can only characterize the near-surface temperature change, the heat generation that occurs deep inside the material is hardly detected by the thermal camera.

Electrical resistance measurement technique can effectively compensate for the limitation of the IR thermography in that it can detect the onset and accumulation of internal defect no matter how thick the studied material is. Since the CNT percolation network is established in all parts of the inspected material, the internal damage formation, regardless of its location, can be sensed by monitoring the increase in the electrical resistance of the material. Studies have also shown that this methodology is particularly effective for characterizing the moment of damage initiation in a material, which can also be considered as the moment when the plastic deformation mode begins [169, 170]. As it can be seen in Figure 10.b, the abrupt increase in electrical resistance seen at the border of deformation stage I and II can be considered as the moment of onset of damage in the material, which is hardly spotted from the stress-strain curve. However, a limitation of electrical resistance measurement method is that it is only applicable to non-conducting materials that has percolation network of conductive fillers, such as CNT doped nanocomposites, carbon black dope composites, and carbon fiber reinforced composites. In addition, a simple electrical resistance measurement does not provide the information about the spatial distribution of the damage, so that characterizing the location of a damage is not feasible.

4.2) Coupled health monitoring system

In the research conducted by Park, K. et al. in 2020, a coupled health monitoring system in which IR thermography and electrical resistance measurements are simultaneously adopted for monitoring the damage state of a composite material [29]. This coupled system is employed in order to compensate the limitations of each technique by the other technique so that a precise evaluation of both the onset and the spatial distribution of damage in composite material can be possible. They performed a uniaxial tensile test of a CNT-doped GFRP, during which the sample is scanned with an IR camera and the electrical resistance of the sample is monitored (Figure 10.a). With the thermal video they obtained with IR camera, the locations of internal damage formation were effectively characterized. Also, the electrical resistance measurement allowed them to detect the formation of damage inside the material.

The result of this static test under coupled health monitoring can be seen in Figure 10.b. Based on three curves recorded during the deformation and the failure process of the sample, they could divide the entire deformation timeline into 3 stages; I) linear elasticity of the material, II) onset of the microdamages, and III) macro-scale crack propagation. Based on the three stages defined on the grid, they could also define a characteristic stress value named Damage stress (σ_D), the stress value at which the transition from stage I to stage II occurs. Since the first and second stage indicate elastic deformation and formation of damage, respectively, the damage stress can be interpreted as the stress value at which the very first damage is nucleated in the material's microstructure. Previous researches have depicted that the damage stresses of various composite materials display good agreement with the fatigue strengths of the material [26, 171, 172]. Therefore, the simultaneous application of IR thermography and electrical resistance measurement has shown a potential for the detection of internal damage and rapid estimation of the fatigue strength of composite materials doped with conductive fillers.

5. Conclusion

In this review, we presented the application of electrical resistance measurement and IR thermography as a structural damage detection technique for composite materials. The operating principles of the two techniques were introduced and some recent research highlights on each of the two NDT methodologies were reviewed. Furthermore, recent advancement in the field of active IR thermography, including optical thermography, laser thermography and eddy current thermography are reported. Regarding the electrical resistance measurement, some recent research results associated with the application of electrical impedance tomography (EIT) for the detection of damage in composite materials are reviewed. At last, the two NDT methods were compared against each other based on their strengths and limitations, and a recent research result regarding the coupling of the two methods for improved damage detection and rapid estimation of fatigue property is discussed.

Figures

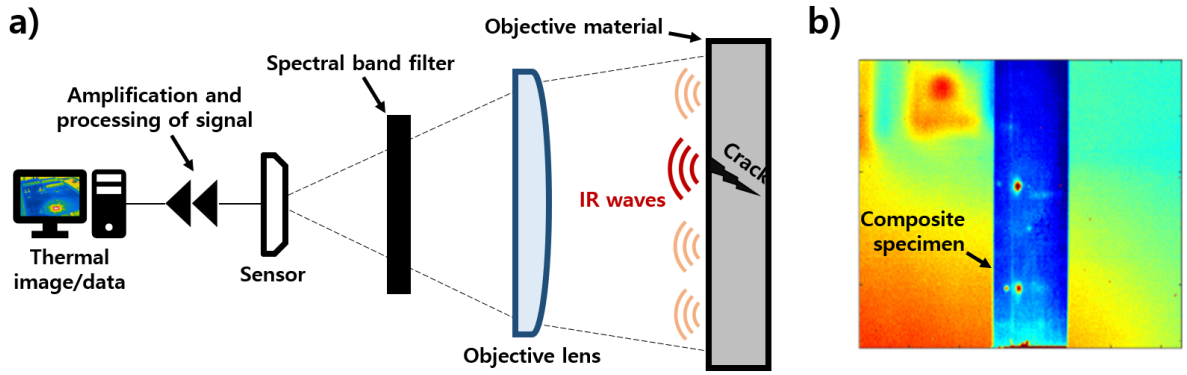

Figure 1. Operating principle of infrared thermography.

(a) Schematic diagram of infrared camera.

(b) A typical thermographic image of a composite specimen under uniaxial tensile test [29]

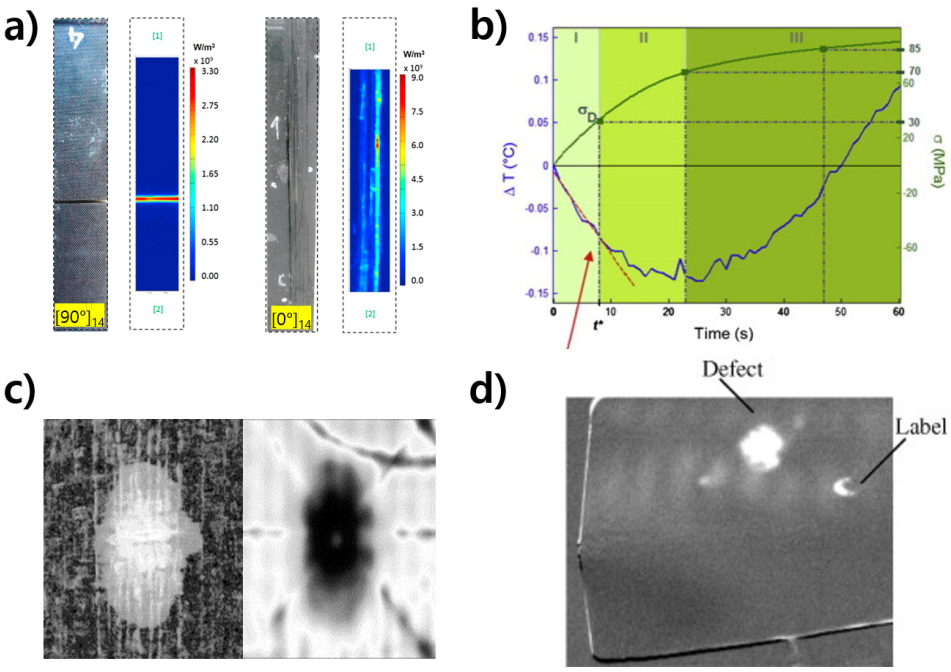

Figure 2. Research results associated with IR thermography as a damage detection technique

(a) Detection of internal damage formation in CFRP via passive IR thermography; $[90°]_{14}$ and $[0°]_{14}$. [38]

(b) A typical average temperature change of a GFRP specimen under uniaxial tensile test captured by passive IR thermography. [26]

(c) Delamination in GFRP captured via active IR thermography with thermal stimulus. [39]

(d) Defect in CFRP, from real wing frame of an aerial vehicle, is detected via ultrasonic IR thermography [53]

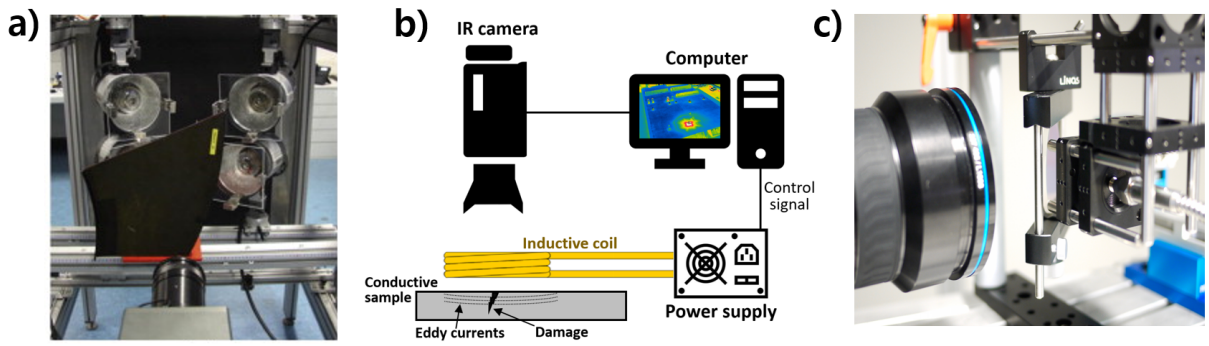

Figure 3. Modern active IR thermography techniques

(a) Application of flash thermography for internal damage inspection. [173]

(b) Schematic diagram of operating principle of eddy current thermography.

(c) Laser thermography. [174]

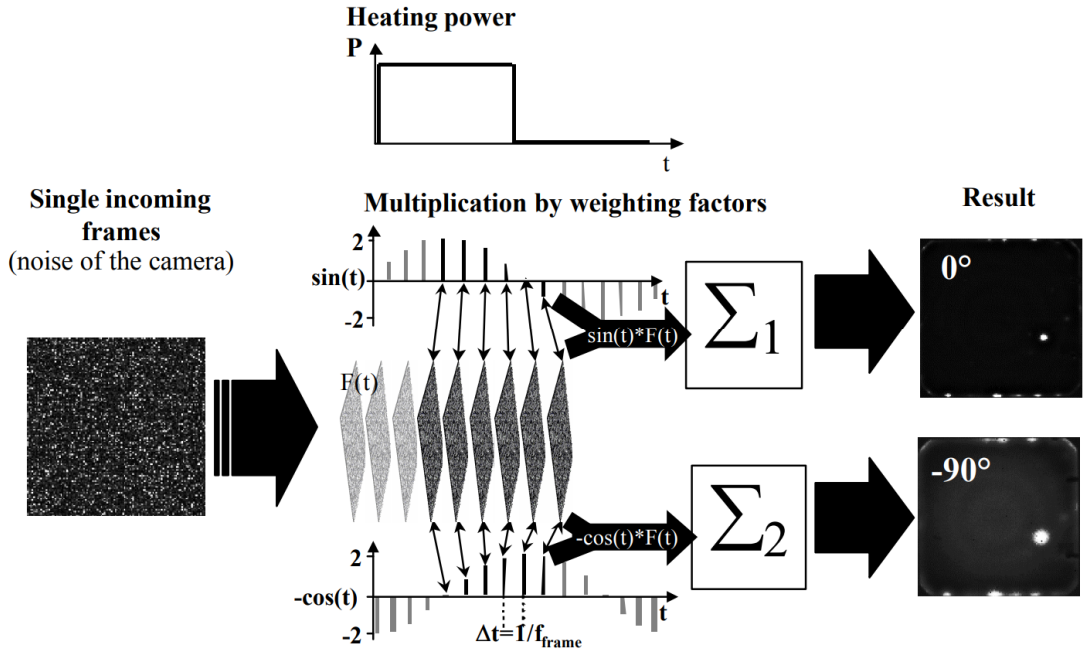

Figure 4. Principle of lock-in IR-thermography [71]

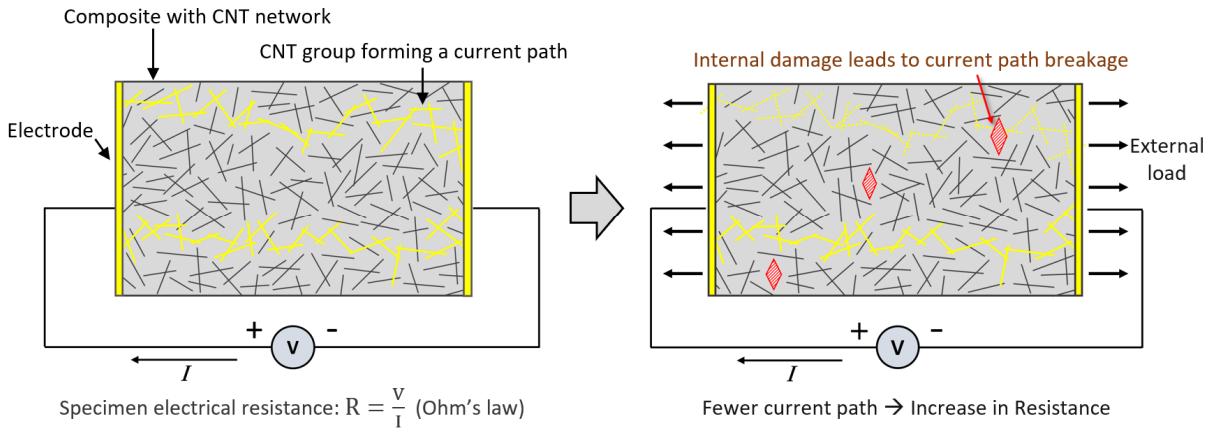

Figure 5. Schematic diagram of electrical resistance measurement for detection of damage in materials. [29]

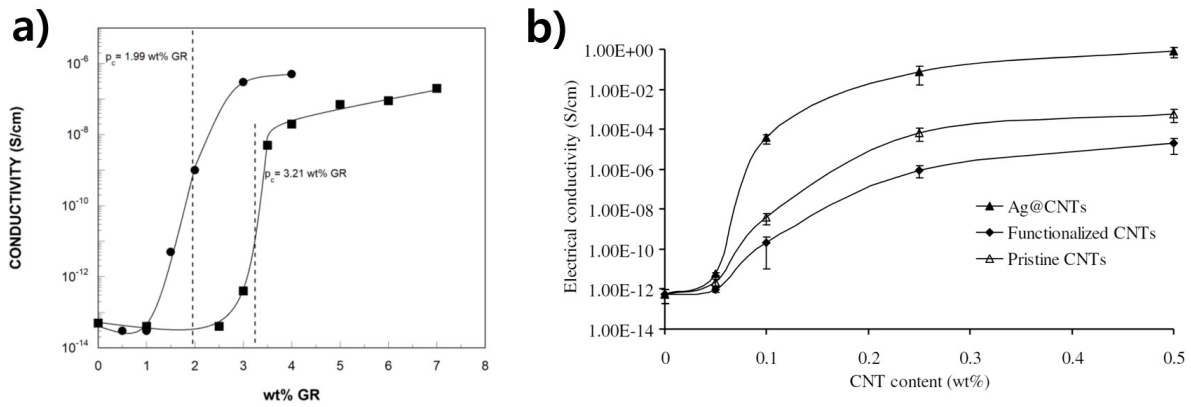

Figure 6. Electrical conductivity of carbon-based nanoparticle-doped composites varied with the particle content

(a) Electrical conductivity of the biobased thermoplastic polyurethane/unmodified graphene nanocomposite (■) and biobased thermoplastic polyurethane/graphene modified with ionic liquid (●) as a function of the graphene content. [175]

(b) Electrical conductivity of CNT-doped epoxy nanocomposite as a function of the CNT content. [176]

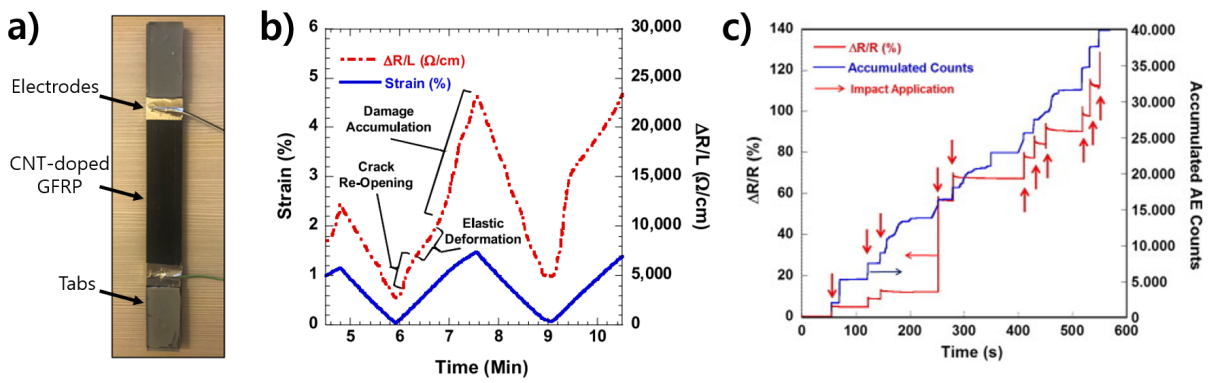

Figure 7. Application of electrical resistance measurement method for the sensing of damage in composite materials.

(a) A CNT-dope GFRP specimen for uniaxial tensile test. The two electrodes built at each end of the specimen is for the electrical resistance measurement. [29]

(b) Electrical resistance trend during the cyclic loading of a specimen. Non-linearity analysis is conducted in order to determine whether the increase in resistance is due to re-opening of an existing crack or formation of a new crack. [75]

(c) A coupled study of electrical resistance change and accumulated acoustic emission (AE) counts during repeated impact loadings. [76]

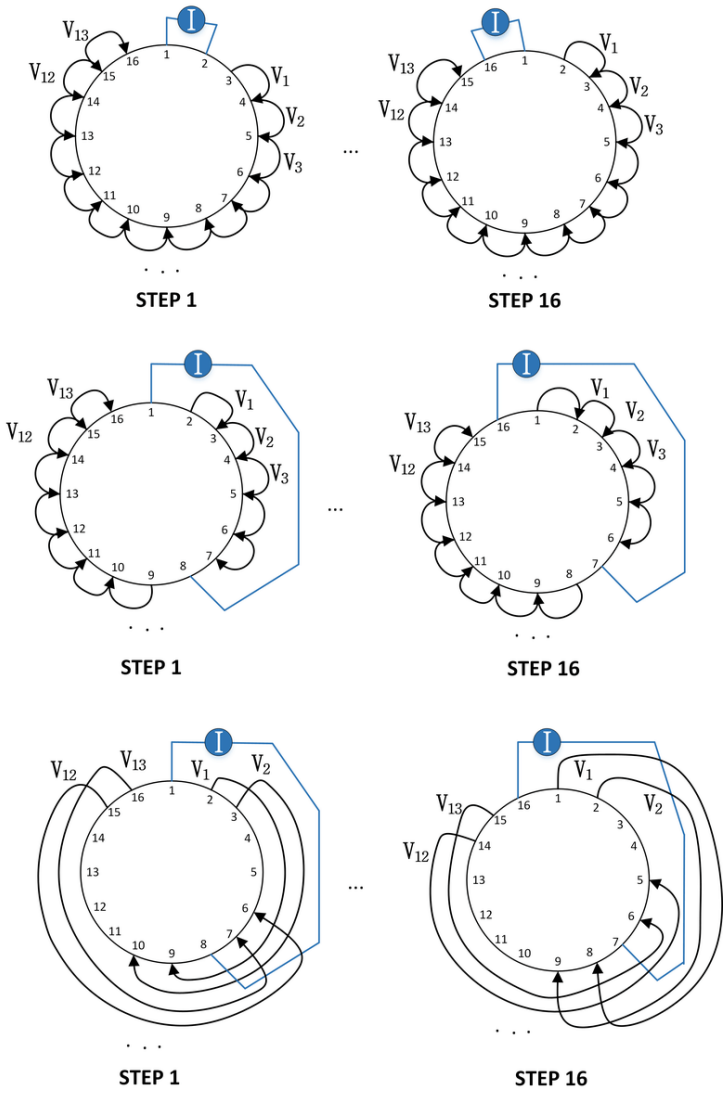

Figure 8. Examples of drive patterns for collection of data. [177]

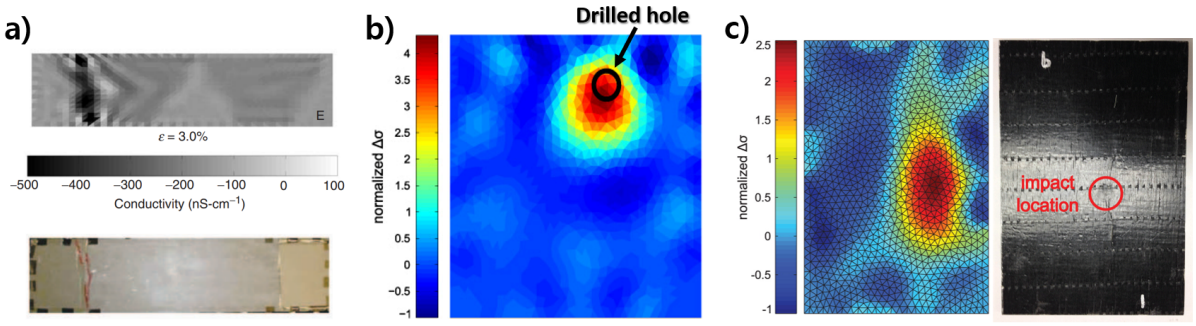

Figure 9. Application of electrical impedance tomography (EIT) for the inspection of defect in carbonaceous filler-doped materials

(a) Reconstructed image of structural damage in cementitious material under monotonic tensile loading. [155]

(b) Reconstructed image of damage detection. The black circle indicates the size and location of actual hole drilled into the material. [159]

(c) Reconstructed image of damage detection. The red circle indicates the location of impact loading applied to the material. [131]

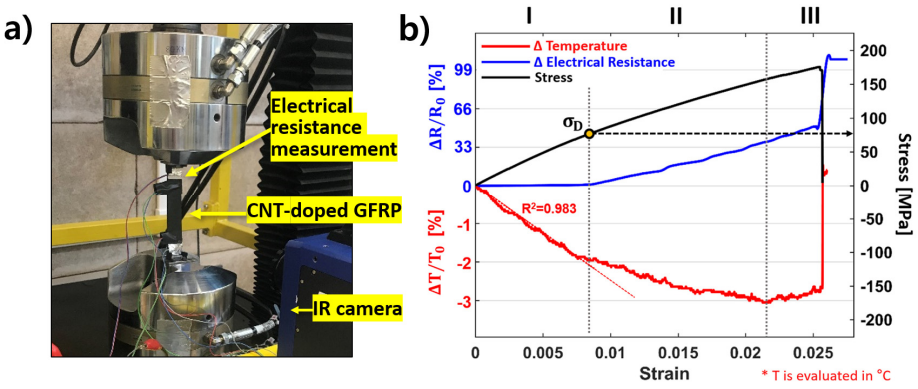

Figure 10. Simultaneous application of electrical resistance measurement and IR camera on damage detection [29]

(a) Uniaxial tensile test of a CNT-doped GFRP specimen under electrical resistance measurement and IR thermography.

(b) Result of the tensile test. Black curve indicates the stress-strain curve. Red curve indicates the average temperature change. Blue curve indicates the change in electrical resistance of the sample. The yellow dot indicates the 'Damage stress'.

Carbon-based nanomaterials	Specific gravity $[g\ cm^{-3}]$	Stiffness $[GPa]$	Strength $[GPa]$	Electrical conductivity $[S\ cm^{-1}]$	Electron mobility $[cm^2v^{-1}s^{-1}]$	Thermal conductivity $[Wm^{-1}K^{-1}]$	Coefficient of linear thermal expansion $[K^{-1}]$
SWCNT	0.8	~1000	13-53	10^2-10^6	10^5	6000	Negligible
MWCNT	1.8	400-4000	63	10^3-10^5	10^4-10^5	2000	Negligible
Graphene	0.763	~1000	130	$1.7 \cdot 10^5$	$2.5 \cdot 10^5$	3000-5000	$-4.8 \cdot 10^{-6}$[a]
Graphite	1.9-2.3	4.1-27.6	4.8-76 MPa	4000[a], 3.3[b]	$2 \cdot 10^4$	298[a], 2.2[b]	$-1 \cdot 10^{-6}$[a], $2.9 \cdot 10^{-5}$[b]
Fullerene	1.7	-	-	10^{-2}-10^{-15}	0.5-6	0.4	$1 \cdot 10^{-6}$-$3 \cdot 10^{-6}$

Table 1. mechanical and multiphysical properties of carbon-based nanomaterials [178-184]

	IR thermography	Electrical resistance measurement
Strength	• Large inspection area • Possible to locate the damaged spot • Applicable to wide range of materials • Results are relatively easy to interpret	• Can detect the formation of internal damage (regardless of the position and size of the crack) • Effectively characterizes the moment of onset of irreversible damage *(elastic → plastic transition)*
Weakness	• Can only detect near-surface damages • Can only detect the damages that result in significant temperature change (e.g. cracks that release enough elastic energy)	• Only applicable to non-conductive materials that has conductive percolation network embedded • Cannot characterize the location of damage unless EIT and appropriate signal processing is applied

Table 2. Strengths and weaknesses of IR thermography and electrical resistance measurement as a damage detection technique.

Reference

1. Chung, D.D., *Composite materials: science and applications*. 2010: Springer Science & Business Media.
2. Clyne, T. and D. Hull, *An introduction to composite materials*. 2019: Cambridge university press.
3. Christensen, R.M., *Mechanics of composite materials*. 2012: Courier Corporation.
4. Giordano, M., et al., *An acoustic-emission characterization of the failure modes in polymer-composite materials.* Composites science and technology, 1998. **58**(12): p. 1923-1928.
5. Sih, G. and E. Chen, *Fracture analysis of unidirectional composites.* Journal of Composite Materials, 1973. **7**(2): p. 230-244.
6. Beaumont, P.W.R., *FRACTURE MECHANISMS IN FIBROUS COMPOSITES*, in *Fracture Mechanics*, R.A. Smith, Editor. 1979, Pergamon. p. 211-233.
7. Talreja, R., *Fatigue of Composite Materials*. 2003. p. 281-294.
8. Harris, B., *Fatigue in composites: science and technology of the fatigue response of fibre-reinforced plastics*. 2003: Woodhead Publishing.
9. Spillman Jr, W. *Fiber optic sensors for composite monitoring*. in *Fiber Optic Smart Structures and Skins*. 1989. International Society for Optics and Photonics.
10. Fish, J., *Multiscale Modeling and Simulation of Composite Materials and Structures*, in *Multiscale Methods in Computational Mechanics: Progress and Accomplishments*, R. de Borst and E. Ramm, Editors. 2011, Springer Netherlands: Dordrecht. p. 215-231.
11. Ko, J. and Y.Q. Ni, *Technology developments in structural health monitoring of large-scale bridges.* Engineering structures, 2005. **27**(12): p. 1715-1725.
12. Abdo, M., *Structural health monitoring, history, applications and future.* A review book. Open Science, 2014.
13. Chang, F.-K., *Structural Health Monitoring: A Summary Report on the First Stanford Workshop on Structural Health Monitoring, September 18-20, 1997*. 1998, STANFORD UNIV CA.
14. Kessler, S.S., *Piezoelectric-based in-situ damage detection of composite materials for structural health monitoring systems*. 2002, Massachusetts Institute of Technology.
15. Mitsheal, A., -Daerefa-a, et al., *A Review of Structural Health Monitoring Techniques as Applied to Composite Structures.* Structural Durability ₩& Health Monitoring, 2017. **11**(2): p. 91--147.
16. Tian, G.Y., et al., *Pulsed Eddy Current Thermography and Applications*, in *New Developments in Sensing Technology for Structural Health Monitoring*, S.C. Mukhopadhyay, Editor. 2011, Springer Berlin Heidelberg: Berlin, Heidelberg. p. 205-231.
17. Meola, C., *Infrared thermography recent advances and future trends*. 2012: Bentham Science Publishers.

18. Prakash, R., *Infrared thermography*. 2012: BoD–Books on Demand.
19. Bagavathiappan, S., et al., *Infrared thermography for condition monitoring–A review.* Infrared Physics & Technology, 2013. **60**: p. 35-55.
20. Meola, C. and G.M. Carlomagno, *Recent advances in the use of infrared thermography.* Measurement Science and Technology, 2004. **15**(9): p. R27-R58.
21. Speakman, J.R. and S. Ward, *Infrared thermography: principles and applications.* Zoology-Jena-, 1998. **101**: p. 224-232.
22. Jo, Y., C. Lee, and J.H. Yoo, *Study on Applicability of Passive Infrared Thermography Analysis for Blistering Detection of Stone Cultural Heritage.* Journal of the Korean Conservation Science for Cultural Properties, 2013. **29**.
23. Planck, M., *The theory of heat radiation*. 2013: Courier Corporation.
24. Tran, Q.H., et al., *Effects of ambient temperature and relative humidity on subsurface defect detection in concrete structures by active thermal imaging.* Sensors, 2017. **17**(8): p. 1718.
25. Martiny, M., et al. *In situ calibration for quantitative infrared thermography*. in *QIRT*. 1996.
26. Libonati, F. and L. Vergani, *Damage assessment of composite materials by means of thermographic analyses.* Composites Part B: Engineering, 2013. **50**: p. 82-90.
27. Pitarresi, G. and E. Patterson, *A review of the general theory of thermoelastic stress analysis.* The Journal of Strain Analysis for Engineering Design, 2003. **38**(5): p. 405-417.
28. Stanley, P. and W. Chan, *The application of thermoelastic stress analysis techniques to composite materials.* The Journal of Strain Analysis for Engineering Design, 1988. **23**(3): p. 137-143.
29. Park, K., et al., *Coupled health monitoring system for CNT-doped self-sensing composites.* Carbon, 2020. **166**: p. 193-204.
30. Vergani, L., C. Colombo, and F. Libonati, *A review of thermographic techniques for damage investigation in composites.* Fract. Struct. Integr. Ann, 2014. **8**.
31. Zalameda, J. and W. Winfree, *Detection and characterization of damage in quasi-static loaded composite structures using passive thermography.* Sensors, 2018. **18**(10): p. 3562.
32. Steinberger, R., et al., *Infrared thermographic techniques for non-destructive damage characterization of carbon fibre reinforced polymers during tensile fatigue testing.* International Journal of Fatigue, 2006. **28**(10): p. 1340-1347.
33. Talreja, R. and C.V. Singh, *Damage and failure of composite materials*. 2012: Cambridge University Press.
34. Wiecek, B. *Review on thermal image processing for passive and active thermography.* in *2005 IEEE Engineering in Medicine and Biology 27th Annual Conference*. 2006. IEEE.
35. Favro, L.D., et al. *IR imaging of cracks excited by an ultrasonic pulse*. in *Thermosense XXII*. 2000. International Society for Optics and Photonics.
36. Gleiter, A., et al., *Ultrasound lock-in thermography for advanced depth resolved defect selective imaging.* Insight-Non-Destructive Testing and Condition Monitoring, 2007. **49**(5): p. 272.

37. Harizi, W., et al., *Mechanical damage assessment of Glass Fiber-Reinforced Polymer composites using passive infrared thermography.* Composites Part B: Engineering, 2014. **59**: p. 74-79.
38. Munoz, V., et al., *Damage detection in CFRP by coupling acoustic emission and infrared thermography.* Composites Part B: Engineering, 2016. **85**: p. 68-75.
39. Guillaumat, L., J.C. Batsale, and D. Mourand, *Real time infra-red image processing for the detection of delamination in composite plates.* Composites Part A: Applied Science and Manufacturing, 2004. **35**(7): p. 939-944.
40. Roche, J.-M., et al., *Passive and active thermography for in situ damage monitoring in woven composites during mechanical testing.* AIP Conference Proceedings, 2013. **1511**(1): p. 555-562.
41. Dattoma, V., et al., *Thermographic investigation of sandwich structure made of composite material.* NDT & E International, 2001. **34**(8): p. 515-520.
42. Shepard, S.M. *Flash thermography of aerospace composites*. in *IV Conferencia Panamericana de END Buenos Aires*. 2007. Citeseer.
43. Toscano, C., et al., *Porosity and inclusion detection in CFRP by infrared thermography.* Advances in Optical Technologies, 2012. **2012**.
44. Poelman, G., et al., *Adaptive spectral band integration in flash thermography: Enhanced defect detectability and quantification in composites.* Composites Part B: Engineering, 2020. **202**: p. 108305.
45. Chen, C.-H., *Ultrasonic and advanced methods for nondestructive testing and material characterization*. 2007: World Scientific.
46. Guo, X. and V. Vavilov, *Crack detection in aluminum parts by using ultrasound-excited infrared thermography.* Infrared Physics & Technology, 2013. **61**: p. 149-156.
47. Vavilov, V., W. Świderski, and D. Derusova, *Ultrasonic and optical stimulation in IR thermographic NDT of impact damage in carbon composites.* Quantitative InfraRed Thermography Journal, 2015. **12**(2): p. 162-172.
48. Shepard, S.M., T. Ahmed, and J.R. Lhota. *Experimental considerations in vibrothermography.* in *Thermosense XXVI*. 2004. International Society for Optics and Photonics.
49. Pieczonka, Ł., M. Szwedo, and T. Uhl, *Vibrothermography-measurement system development and testing.* Diagnostyka, 2011: p. 61-66.
50. Han, X., et al., *Acoustic chaos and sonic infrared imaging.* Applied Physics Letters, 2002. **81**(17): p. 3188-3190.
51. Rantala, J., et al. *Lock-in thermography with mechanical loss angle heating at ultrasonic frequencies*. in *Proc. Int Conf. Quantitative InfraRed Thermography (QIRT96)*. 1996.
52. Umar, M.Z., et al., *Ultrasonic infrared thermography in non-destructive testing: A review.* Russian Journal of Nondestructive Testing, 2016. **52**(4): p. 212-219.
53. Yang, B., Y. Huang, and L. Cheng, *Defect detection and evaluation of ultrasonic infrared thermography for aerospace CFRP composites.* Infrared Physics & Technology, 2013. **60**: p.

166-173.
54. Zenzinger, G., et al., *Thermographic crack detection by eddy current excitation.* Nondestructive Testing and Evaluation, 2007. **22**(2-3): p. 101-111.
55. Tian, G.Y., et al., *Eddy Current Pulsed Thermography with Different Excitation Configurations for Metallic Material and Defect Characterization.* Sensors, 2016. **16**(6): p. 843.
56. Wilson, J., et al., *Pulsed eddy current thermography: system development and evaluation.* Insight-Non-Destructive Testing and Condition Monitoring, 2010. **52**(2): p. 87-90.
57. Li, T., D.P. Almond, and D.A.S. Rees, *Crack imaging by scanning pulsed laser spot thermography.* NDT & E International, 2011. **44**(2): p. 216-225.
58. Yang, R. and Y. He, *Optically and non-optically excited thermography for composites: A review.* Infrared Physics & Technology, 2016. **75**: p. 26-50.
59. Wu, D. and G. Busse, *Lock-in thermography for nondestructive evaluation of materials.* Revue Générale de Thermique, 1998. **37**(8): p. 693-703.
60. Riegert, G., T. Zweschper, and G. Busse, *Lockin thermography with eddy current excitation.* Quantitative InfraRed Thermography Journal, 2004. **1**(1): p. 21-32.
61. Oswald-Tranta, B. and G. Wally. *Thermo-inductive surface crack detection in metallic materials*. in *Proc. 9th Eur. Conf. NDT*. 2006.
62. Walle, G. and U. Netzelmann, *Thermographic crack detection in ferritic steel components using inductive heating.* Proc. 9th ECNDT Berlin, 2006. **25**(29.9).
63. Wu, J., et al., *DC-Biased Magnetization Based Eddy Current Thermography for Subsurface Defect Detection.* IEEE Transactions on Industrial Informatics, 2019. **15**(12): p. 6252-6259.
64. Schlichting, J., C. Maierhofer, and M. Kreutzbruck, *Crack sizing by laser excited thermography.* NDT & E International, 2012. **45**(1): p. 133-140.
65. He, Z., et al., *Joint scanning laser thermography defect detection method for carbon fiber reinforced polymer.* IEEE Sensors Journal, 2019. **20**(1): p. 328-336.
66. Roemer, J., T. Uhl, and L. Pieczonka. *Laser spot thermography for crack detection in aluminum structures*. in *7th International Symposium on NDT in Aerospace*. 2015.
67. Li, T., D.P. Almond, and D.A.S. Rees, *Crack imaging by scanning laser-line thermography and laser-spot thermography.* Measurement Science and Technology, 2011. **22**(3): p. 035701.
68. Vavilov, V.P. and D.D. Burleigh, *Review of pulsed thermal NDT: Physical principles, theory and data processing.* Ndt & E International, 2015. **73**: p. 28-52.
69. Cerniglia, D. and N. Montinaro, *Defect Detection in Additively Manufactured Components: Laser Ultrasound and Laser Thermography Comparison.* Procedia Structural Integrity, 2018. **8**: p. 154-162.
70. Meola, C., et al., *Non-destructive evaluation of aerospace materials with lock-in thermography.* Engineering failure analysis, 2006. **13**(3): p. 380-388.
71. Huth, S., et al. *Lock-in IR-thermography-A novel tool for material and device characterization*. in *diffusion and defect data part B solid state phenomena*. 2002. Citeseer.
72. Breitenstein, O. and M. Langenkamp, *Lock-in thermography*, in *Basics and Use for Functional*

Diagnostics of Electronics Components. 2003, Springer.
73. Baughman, R.H., et al., *Carbon nanotube actuators.* Science, 1999. **284**(5418): p. 1340-1344.
74. Spinks, G.M., et al. *Conducting polymers electromechanical actuators and strain sensors*. in *Macromolecular Symposia*. 2003. Wiley Online Library.
75. Thostenson, E.T. and T.-W. Chou, *Real-time in situ sensing of damage evolution in advanced fiber composites using carbon nanotube networks.* Nanotechnology, 2008. **19**(21): p. 215713.
76. Gao, L., et al., *In situ sensing of impact damage in epoxy/glass fiber composites using percolating carbon nanotube networks.* Carbon, 2011. **49**(10): p. 3382-3385.
77. Liu, S., et al., *A review of extending performance of epoxy resins using carbon nanomaterials.* Composites Part B: Engineering, 2018. **136**: p. 197-214.
78. Choudhary, N., S. Hwang, and W. Choi, *Carbon nanomaterials: a review.* Handbook of nanomaterials properties, 2014: p. 709-769.
79. Yee, M.J., et al., *Carbon nanomaterials based films for strain sensing application—A review.* Nano-Structures & Nano-Objects, 2019. **18**: p. 100312.
80. Qu, S., et al., *Carbon nanotube film based multifunctional composite materials: an overview.* Functional Composites and Structures, 2020. **2**(2): p. 022002.
81. Thostenson, E.T., Z. Ren, and T.-W. Chou, *Advances in the science and technology of carbon nanotubes and their composites: a review.* Composites science and technology, 2001. **61**(13): p. 1899-1912.
82. Ajayan, P.M., L.S. Schadler, and P.V. Braun, *Nanocomposite science and technology*. 2006: John Wiley & Sons.
83. Coleman, J.N., U. Khan, and Y.K. Gun'ko, *Mechanical reinforcement of polymers using carbon nanotubes.* Advanced materials, 2006. **18**(6): p. 689-706.
84. Saleh, N.B., L.D. Pfefferle, and M. Elimelech, *Influence of biomacromolecules and humic acid on the aggregation kinetics of single-walled carbon nanotubes.* Environmental science & technology, 2010. **44**(7): p. 2412-2418.
85. Girifalco, L.A., M. Hodak, and R.S. Lee, *Carbon nanotubes, buckyballs, ropes, and a universal graphitic potential.* Physical Review B, 2000. **62**(19): p. 13104.
86. Li, D., et al., *Processable aqueous dispersions of graphene nanosheets.* Nature nanotechnology, 2008. **3**(2): p. 101-105.
87. Yazdani, H., B.E. Smith, and K. Hatami, *Multi-walled carbon nanotube-filled polyvinyl chloride composites: Influence of processing method on dispersion quality, electrical conductivity and mechanical properties.* Composites Part A: Applied Science and Manufacturing, 2016. **82**: p. 65-77.
88. Li, J., et al., *Correlations between percolation threshold, dispersion state, and aspect ratio of carbon nanotubes.* Advanced Functional Materials, 2007. **17**(16): p. 3207-3215.
89. Chang, L., et al., *Evaluation and visualization of the percolating networks in multi-wall carbon nanotube/epoxy composites.* Journal of Materials Science, 2009. **44**(15): p. 4003-4012.
90. Rana, S., R. Alagirusamy, and M. Joshi, *A review on carbon epoxy nanocomposites.* Journal

of Reinforced Plastics and Composites, 2009. **28**(4): p. 461-487.
91. Qian, D., et al., *Load transfer and deformation mechanisms in carbon nanotube-polystyrene composites.* Applied physics letters, 2000. **76**(20): p. 2868-2870.
92. Sandler, J., et al., *Development of a dispersion process for carbon nanotubes in an epoxy matrix and the resulting electrical properties.* Polymer, 1999. **40**(21): p. 5967-5971.
93. Ma, P.-C., et al., *Dispersion and functionalization of carbon nanotubes for polymer-based nanocomposites: a review.* Composites Part A: Applied Science and Manufacturing, 2010. **41**(10): p. 1345-1367.
94. Polo-Luque, M., B. Simonet, and M. Valcárcel, *Functionalization and dispersion of carbon nanotubes in ionic liquids.* TrAC Trends in Analytical Chemistry, 2013. **47**: p. 99-110.
95. Zhou, L., et al., *Multi-walled carbon nanotubes: a cytotoxicity study in relation to functionalization, dose and dispersion.* Toxicology In Vitro, 2017. **42**: p. 292-298.
96. Mickelson, E., et al., *Fluorination of single-wall carbon nanotubes.* Chemical physics letters, 1998. **296**(1-2): p. 188-194.
97. Touhara, H., et al., *Fluorination of cup-stacked carbon nanotubes, structures and properties.* MRS Online Proceedings Library, 2004. **858**(1): p. 40-45.
98. Zhang, Q.-H. and D.-J. Chen, *Percolation threshold and morphology of composites of conducting carbon black/polypropylene/EVA.* Journal of materials science, 2004. **39**(5): p. 1751-1757.
99. Chen, J., et al., *Solution properties of single-walled carbon nanotubes.* Science, 1998. **282**(5386): p. 95-98.
100. Holzinger, M., et al., *[2+ 1] cycloaddition for cross-linking SWCNTs.* Carbon, 2004. **42**(5-6): p. 941-947.
101. Kim, K.S., et al., *Modification of electronic structures of a carbon nanotube by hydrogen functionalization.* Advanced Materials, 2002. **14**(24): p. 1818-1821.
102. Mitchell, C.A., et al., *Dispersion of functionalized carbon nanotubes in polystyrene.* Macromolecules, 2002. **35**(23): p. 8825-8830.
103. Loh, K.P., et al., *The chemistry of graphene.* Journal of Materials Chemistry, 2010. **20**(12): p. 2277-2289.
104. Jin, F.-L., X. Li, and S.-J. Park, *Synthesis and application of epoxy resins: A review.* Journal of Industrial and Engineering Chemistry, 2015. **29**: p. 1-11.
105. Montserrat, S. and J. Málek, *A kinetic analysis of the curing reaction of an epoxy resin.* Thermochimica acta, 1993. **228**: p. 47-60.
106. Li, C. and T.-W. Chou, *Modeling of damage sensing in fiber composites using carbon nanotube networks.* Composites Science and Technology, 2008. **68**(15): p. 3373-3379.
107. Wang, Y. and G.J. Weng, *Electrical conductivity of carbon nanotube-and graphene-based nanocomposites*, in *Micromechanics and Nanomechanics of Composite Solids*. 2018, Springer. p. 123-156.
108. Xia, Z. and W. Curtin, *Modeling of mechanical damage detection in CFRPs via electrical*

resistance. Composites science and technology, 2007. **67**(7-8): p. 1518-1529.
109. Tumanski, S., *Principles of electrical measurement*. 2006: CRC press.
110. Badr, J., et al., *Design and validation of a multi-electrode embedded sensor to monitor resistivity profiles over depth in concrete.* Construction and Building Materials, 2019. **223**: p. 310-321.
111. Douville, N.J., et al., *Fabrication of Two-Layered Channel System with Embedded Electrodes to Measure Resistance Across Epithelial and Endothelial Barriers.* Analytical Chemistry, 2010. **82**(6): p. 2505-2511.
112. Baltopoulos, A., et al., *Exploiting carbon nanotube networks for damage assessment of fiber reinforced composites.* Composites Part B: Engineering, 2015. **76**: p. 149-158.
113. Dai, H., et al., *A Novel Methodology for Spatial Damage Detection and Imaging Using a Distributed Carbon Nanotube-Based Composite Sensor Combined with Electrical Impedance Tomography.* Journal of Nondestructive Evaluation, 2016. **35**(2): p. 26.
114. Sham, M.L., et al., *Cleaning and functionalization of polymer surfaces and nanoscale carbon fillers by UV/ozone treatment: a review.* Journal of composite materials, 2009. **43**(14): p. 1537-1564.
115. Zhang, W., A.A. Dehghani-Sanij, and R.S. Blackburn, *Carbon based conductive polymer composites.* Journal of materials science, 2007. **42**(10): p. 3408-3418.
116. Li, J., et al., *Morphology and properties of UV/ozone treated graphite nanoplatelet/epoxy nanocomposites.* Composites Science and Technology, 2007. **67**(2): p. 296-305.
117. Ma, P.C., J.-K. Kim, and B.Z. Tang, *Effects of silane functionalization on the properties of carbon nanotube/epoxy nanocomposites.* Composites Science and Technology, 2007. **67**(14): p. 2965-2972.
118. Sandler, J., et al., *Ultra-low electrical percolation threshold in carbon-nanotube-epoxy composites.* Polymer, 2003. **44**(19): p. 5893-5899.
119. Martin, C., et al., *Electric field-induced aligned multi-wall carbon nanotube networks in epoxy composites.* Polymer, 2005. **46**(3): p. 877-886.
120. Bauhofer, W. and J.Z. Kovacs, *A review and analysis of electrical percolation in carbon nanotube polymer composites.* Composites science and technology, 2009. **69**(10): p. 1486-1498.
121. Gao, L., et al., *A comparative study of damage sensing in fiber composites using uniformly and non-uniformly dispersed carbon nanotubes.* Carbon, 2010. **48**(13): p. 3788-3794.
122. Stankovich, S., et al., *Graphene-based composite materials.* Nature, 2006. **442**(7100): p. 282-286.
123. Zha, J.-W., et al., *High-performance strain sensors based on functionalized graphene nanoplates for damage monitoring.* Composites Science and Technology, 2016. **123**: p. 32-38.
124. Balaji, R. and M. Sasikumar, *Graphene based strain and damage prediction system for polymer composites.* Composites Part A: Applied Science and Manufacturing, 2017. **103**: p.

48-59.

125. Hao, B., et al., *Comparative study on monitoring structural damage in fiber-reinforced polymers using glass fibers with carbon nanotubes and graphene coating.* Composites Science and Technology, 2016. **129**: p. 38-45.
126. Groo, L., et al., *Laser induced graphene in fiberglass-reinforced composites for strain and damage sensing.* Composites Science and Technology, 2020. **199**: p. 108367.
127. Groo, L., et al., *Laser induced graphene for in situ damage sensing in aramid fiber reinforced composites.* Composites Science and Technology, 2021. **201**: p. 108541.
128. Huang, J.C., *Carbon black filled conducting polymers and polymer blends.* Advances in Polymer Technology: Journal of the Polymer Processing Institute, 2002. **21**(4): p. 299-313.
129. Gopi, J.A., et al., *SBR-clay-carbon black hybrid nanocomposites for tire tread application.* Journal of Polymer Research, 2011. **18**(6): p. 1625-1634.
130. Vadlamani, V.K., et al., *Sensing of damage in carbon nanotubes and carbon black-embedded epoxy under tensile loading.* Polymer Composites, 2012. **33**(10): p. 1809-1815.
131. Tallman, T.N., et al., *Damage detection via electrical impedance tomography in glass fiber/epoxy laminates with carbon black filler.* Structural Health Monitoring, 2015. **14**(1): p. 100-109.
132. Yazdani, H., et al., *Strain-sensitive conductivity of carbon black-filled PVC composites subjected to cyclic loading.* Carbon, 2014. **79**: p. 393-405.
133. Wang, Y., et al., *In Situ Strain and Damage Monitoring of GFRP Laminates Incorporating Carbon Nanofibers under Tension.* Polymers, 2018. **10**(7): p. 777.
134. Wang, Y., et al., *Strain and damage self-sensing of basalt fiber reinforced polymer laminates fabricated with carbon nanofibers/epoxy composites under tension.* Composites Part A: Applied Science and Manufacturing, 2018. **113**: p. 40-52.
135. Monti, M., et al., *Carbon nanofibers for strain and impact damage sensing in glass fiber reinforced composites based on an unsaturated polyester resin.* Polymer Composites, 2011. **32**(5): p. 766-775.
136. Zhang, D., et al., *Assessment of transverse impact damage in GF/EP laminates of conductive nanoparticles using electrical resistivity tomography.* Composites Part A: Applied Science and Manufacturing, 2012. **43**(9): p. 1587-1598.
137. Naghashpour, A. and S. Van Hoa, *A technique for real-time detection, location and quantification of damage in large polymer composite structures made of electrically non-conductive fibers and carbon nanotube networks.* Nanotechnology, 2013. **24**(45): p. 455502.
138. Thomas, A., et al., *Damage detection in self-sensing composite tubes via electrical impedance tomography.* Composites Part B: Engineering, 2019. **177**: p. 107276.
139. Dai, H., et al., *A novel methodology for spatial damage detection and imaging using a distributed carbon nanotube-based composite sensor combined with electrical impedance tomography.* Journal of Nondestructive Evaluation, 2016. **35**(2): p. 1-15.
140. Somersalo, E., M. Cheney, and D. Isaacson, *Existence and uniqueness for electrode models*

for electric current computed tomography. SIAM Journal on Applied Mathematics, 1992. **52**(4): p. 1023-1040.

141. Sylvester, J. and G. Uhlmann, *A uniqueness theorem for an inverse boundary value problem in electrical prospection.* Communications on Pure and Applied Mathematics, 1986. **39**(1): p. 91-112.
142. Vauhkonen, P.J., et al., *Three-dimensional electrical impedance tomography based on the complete electrode model.* IEEE Transactions on Biomedical Engineering, 1999. **46**(9): p. 1150-1160.
143. Kaipio, J.P., et al., *Inverse problems with structural prior information.* Inverse problems, 1999. **15**(3): p. 713.
144. Vauhkonen, M., et al., *Tikhonov regularization and prior information in electrical impedance tomography.* IEEE transactions on medical imaging, 1998. **17**(2): p. 285-293.
145. Cheney, M., et al., *NOSER: An algorithm for solving the inverse conductivity problem.* International Journal of Imaging systems and technology, 1990. **2**(2): p. 66-75.
146. Adler, A. and W.R. Lionheart, *Uses and abuses of EIDORS: an extensible software base for EIT.* Physiological measurement, 2006. **27**(5): p. S25.
147. Eldar, Y.C. and A.V. Oppenheim, *Covariance shaping least-squares estimation.* IEEE Transactions on Signal Processing, 2003. **51**(3): p. 686-697.
148. Olmi, R., M. Bini, and S. Priori, *A genetic algorithm approach to image reconstruction in electrical impedance tomography.* IEEE Transactions on Evolutionary Computation, 2000. **4**(1): p. 83-88.
149. Kumar, S.P., et al. *Reconstruction of brain electrical impedance tomography images using particle swarm optimization*. in *2010 5th International Conference on Industrial and Information Systems*. 2010. IEEE.
150. Li, Y., et al. *Image reconstruction of EIT using differential evolution algorithm*. in *Proceedings of the 25th Annual International Conference of the IEEE Engineering in Medicine and Biology Society (IEEE Cat. No. 03CH37439)*. 2003. IEEE.
151. Lim, S.P. and H. Haron. *Performance comparison of genetic algorithm, differential evolution and particle swarm optimization towards benchmark functions*. in *2013 IEEE Conference on Open Systems (ICOS)*. 2013. IEEE.
152. Hamilton, S.J. and A. Hauptmann, *Deep D-bar: Real-time electrical impedance tomography imaging with deep neural networks.* IEEE transactions on medical imaging, 2018. **37**(10): p. 2367-2377.
153. Hamilton, S.J., et al., *Beltrami-net: domain-independent deep D-bar learning for absolute imaging with electrical impedance tomography (a-EIT).* Physiological measurement, 2019. **40**(7): p. 074002.
154. Park, H., et al. *Deep neural network approach in electrical impedance tomography-based real-time soft tactile sensor*. in *2019 IEEE/RSJ International Conference on Intelligent Robots and Systems (IROS)*. 2019. IEEE.

155. Hou, T.-C. and J.P. Lynch, *Electrical impedance tomographic methods for sensing strain fields and crack damage in cementitious structures.* Journal of Intelligent Material Systems and Structures, 2009. **20**(11): p. 1363-1379.
156. Hallaji, M. and M. Pour-Ghaz, *A new sensing skin for qualitative damage detection in concrete elements: Rapid difference imaging with electrical resistance tomography.* NDT & E International, 2014. **68**: p. 13-21.
157. Hallaji, M., A. Seppänen, and M. Pour-Ghaz, *Electrical impedance tomography-based sensing skin for quantitative imaging of damage in concrete.* Smart Materials and Structures, 2014. **23**(8): p. 085001.
158. Rashetnia, R., et al., *Electrical resistance tomography–based sensing skin with internal electrodes for crack detection in large structures.* Materials Evaluation, 2018. **76**(10): p. 1405-1413.
159. Tallman, T.N., et al., *Damage detection and conductivity evolution in carbon nanofiber epoxy via electrical impedance tomography.* Smart Materials and Structures, 2014. **23**(4): p. 045034.
160. Lestari, W., et al., *Sensing uniaxial tensile damage in fiber-reinforced polymer composites using electrical resistance tomography.* Smart Materials and Structures, 2016. **25**(8): p. 085016.
161. Hou, T.-C., K.J. Loh, and J.P. Lynch, *Spatial conductivity mapping of carbon nanotube composite thin films by electrical impedance tomography for sensing applications.* Nanotechnology, 2007. **18**(31): p. 315501.
162. Loh, K.J., et al., *Carbon nanotube sensing skins for spatial strain and impact damage identification.* Journal of Nondestructive Evaluation, 2009. **28**(1): p. 9-25.
163. Ghaednia, H., et al., *Interfacial load monitoring and failure detection in total joint replacements via piezoresistive bone cement and electrical impedance tomography.* Smart Materials and Structures, 2020. **29**(8): p. 085039.
164. Ghaednia, H., et al., *Is Machine Learning Able to Detect and Classify Failure in Piezoresistive Bone Cement Based on Electrical Signals?* arXiv preprint arXiv:2010.12147, 2020.
165. ZHAO, Y., S. GSCHOSSMANN, and M. SCHAGERL, *Observing the fracture behavior of a center crack via electrical impedance tomography using inkjet-printed carbon nanotube thin films.* Structural Health Monitoring 2017, 2017(shm).
166. Hassan, H. and T.N. Tallman, *Failure prediction in self-sensing nanocomposites via genetic algorithm-enabled piezoresistive inversion.* Structural Health Monitoring, 2020. **19**(3): p. 765-780.
167. Milovanović, B. and I. Banjad Pečur, *Review of active IR thermography for detection and characterization of defects in reinforced concrete.* Journal of Imaging, 2016. **2**(2): p. 11.
168. Kaplan, H., *Practical applications of infrared thermal sensing and imaging equipment*. Vol. 75. 2007: SPIE press.
169. Gao, L., et al., *Coupled carbon nanotube network and acoustic emission monitoring for sensing of damage development in composites*. Carbon, 2009. **47**(5): p. 1381-1388.

170. Ku-Herrera, J.J., et al., *Self-sensing of damage progression in unidirectional multiscale hierarchical composites subjected to cyclic tensile loading*. Sensors, 2016. **16**(3): p. 400.
171. Colombo, C., et al. *Fatigue behaviour of a GFRP laminate by thermographic measurements*. in *11th International Conference on the Mechanical Behavior of Materials (ICM11)*. 2011. Elsevier.
172. Colombo, C., F. Libonati, and L. Vergani, *Fatigue damage in GFRP.* International Journal of Structural Integrity, 2012. **3**(4): p. 424-440.
173. Maierhofer, C., et al., *Characterizing damage in CFRP structures using flash thermography in reflection and transmission configurations.* Composites Part B: Engineering, 2014. **57**: p. 35-46.
174. Esposito, C. *LTvis - designed for fast tests*. 2020; Available from: https://www.edevis.com/content/en/Laser_thermography.php.
175. Aranburu, N., I. Otaegi, and G. Guerrica-Echevarria, *Using an Ionic Liquid to Reduce the Electrical Percolation Threshold in Biobased Thermoplastic Polyurethane/Graphene Nanocomposites.* Polymers, 2019. **11**(3): p. 435.
176. Ma, P.C., B.Z. Tang, and J.-K. Kim, *Effect of CNT decoration with silver nanoparticles on electrical conductivity of CNT-polymer composites.* Carbon, 2008. **46**(11): p. 1497-1505.
177. Russo, S., et al., *A quantitative evaluation of drive pattern selection for optimizing EIT-based stretchable sensors.* Sensors, 2017. **17**(9): p. 1999.
178. Al-Hamadani, Y.A.J., et al., *Stabilization and dispersion of carbon nanomaterials in aqueous solutions: A review.* Separation and Purification Technology, 2015. **156**: p. 861-874.
179. Lu, J.P., *Elastic properties of carbon nanotubes and nanoropes.* Physical Review Letters, 1997. **79**(7): p. 1297.
180. Treacy, M.J., T.W. Ebbesen, and J.M. Gibson, *Exceptionally high Young's modulus observed for individual carbon nanotubes.* nature, 1996. **381**(6584): p. 678-680.
181. Yu, M.-F., et al., *Strength and breaking mechanism of multiwalled carbon nanotubes under tensile load.* Science, 2000. **287**(5453): p. 637-640.
182. Dresselhaus, G., M.S. Dresselhaus, and R. Saito, *Physical properties of carbon nanotubes*. 1998: World scientific.
183. Weiss, N.O., et al., *Graphene: an emerging electronic material.* Advanced materials, 2012. **24**(43): p. 5782-5825.
184. Radamson, H.H., *Graphene*, in *Springer Handbook of Electronic and Photonic Materials*, S. Kasap and P. Capper, Editors. 2017, Springer International Publishing: Cham. p. 1-1.